Journal of *Marine Science and Engineering*

MDPI

Article

It Often Howls More than It Chugs: Wind versus Ship Noise Under Water in Australia's Maritime Regions

Christine Erbe [1,*], Renee P. Schoeman [1], David Peel [2] and Joshua N. Smith [3]

[1] Centre for Marine Science and Technology, Curtin University, Perth, WA 6102, Australia; renee.p.schoeman@gmail.com
[2] Data 61, CSIRO, CSIRO Marine Laboratories, Hobart, TAS 7004, Australia; david.peel@data61.csiro.au
[3] Centre for Sustainable Aquatic Ecosystems, Harry Butler Institute, Murdoch University, Perth, WA 6150, Australia; joshua.smith@uqconnect.edu.au
* Correspondence: c.erbe@curtin.edu.au

Abstract: Marine soundscapes consist of cumulative contributions by diverse sources of sound grouped into: physical (e.g., wind), biological (e.g., fish), and anthropogenic (e.g., shipping)—each with unique spatial, temporal, and frequency characteristics. In terms of anthropophony, shipping has been found to be the greatest (ubiquitous and continuous) contributor of low-frequency underwater noise in several northern hemisphere soundscapes. Our aim was to develop a model for ship noise in Australian waters, which could be used by industry and government to manage marine zones, their usage, stressors, and potential impacts. We also modelled wind noise under water to provide context to the contribution of ship noise. The models were validated with underwater recordings from 25 sites. As expected, there was good congruence when shipping or wind were the dominant sources. However, there was less agreement when other anthropogenic or biological sources were present (i.e., primarily marine seismic surveying and whales). Off Australia, pristine marine soundscapes (based on the dominance of natural, biological and physical sound) remain, in particular, near offshore reefs and islands. Strong wind noise dominates along the southern Australian coast. Underwater shipping noise dominates only in certain areas, along the eastern seaboard and on the northwest shelf, close to shipping lanes.

Keywords: marine soundscape; ship noise; wind noise; whale song; fish chorus; Australian EEZ

Citation: Erbe, C.; Schoeman, R.P.; Peel, D.; Smith, J.N. It Often Howls More than It Chugs: Wind versus Ship Noise Under Water in Australia's Maritime Regions. *J. Mar. Sci. Eng.* **2021**, *9*, 472. https://doi.org/10.3390/jmse9050472

Academic Editor: Michele Viviani

Received: 30 March 2021
Accepted: 25 April 2021
Published: 27 April 2021

1. Introduction

The oceans abound with natural physical sounds (from wind, rain, polar ice, and seismic activity), biological sounds (from crustaceans, fishes, and marine mammals), and anthropogenic sounds (from transport, construction, offshore exploration, and mining). Soundscapes naturally change over time because of temporal cycles in weather (e.g., cyclones and annual monsoon [1,2]) and animal behaviour (e.g., diurnal foraging patterns, lunar spawning, seasonal mating, and annual migration [3–6]). However, in many habitats, soundscapes further change with patterns of human presence (e.g., temporary construction or summer recreation [7]) and some have changed steadily over time with increasing intensity of anthropophony (e.g., due to shipping [8]).

In 1996, the European Commission identified air-borne noise as one of the main terrestrial environmental issues in Europe, having been neglected compared to chemical pollution [9]. Subsequently, the Commission enacted sound mapping as an important step to assess and manage sound exposure levels in urban areas [10]. A little later, the issue of underwater ocean noise received similar attention, being declared a pollutant, and with underwater sound monitoring and mapping being suggested [11]. Nowadays, underwater noise footprints of individual anthropogenic operations are commonly mapped for environmental impact assessments (e.g., [12–14]). Longer-term, large-scale marine

sound mapping has focussed on ship noise [15–17], but may also include other sources, such as seismic airguns and explosives [18].

Shipping is a global contributor to ocean noise and, over the past five decades, has caused a steady increase in underwater low-frequency (10–100 Hz) ambient sound levels in many marine regions [19–24]. This is of concern, because ship noise causes behavioural and acoustic responses, auditory masking, and stress in marine animals [25–28]. Hence, various studies have mapped ship noise and overlain the resulting maps with marine habitat maps to identify areas of concern (hotspots; high animal density and high noise) [29] and areas of opportunity (high animal density and low noise) [30] for marine spatial planning.

A problem with ship noise maps is that they often lack validation against in situ measurements. These maps may have several sources of error in the ship positions and routes, source spectra and levels, sound propagation models, and hydro- and geoacoustic parameters required by the models. As well, the spatial (depth and range) and temporal grid over which the models operate introduces uncertainty. In fact, lack of knowledge on the physical environment (i.e., hydroacoustic parameters of the water and geoacoustic parameters of the upper seafloor) is often the limiting factor in sound propagation model accuracy [14,31]. Model validation is essential to confirm accuracy and to support the use of a sound map for management decisions [32].

Finally, underwater anthropogenic noise needs to be put into context. How does it compare to natural, pervasive noise as from wind? Sertlek et al. [18] found that shipping inserted the greatest amount of acoustic energy into the Dutch North Sea and far exceeded that of wind. Similarly, Farcas et al. [32] showed that ship noise exceeded wind noise under water near major ports and shipping lanes, and around industrial sites in the Northeast Atlantic. However, southern hemisphere oceans have a reputation of being less impacted by anthropogenic sounds, largely due to a lower ship density [33]. Thus, wind may supersede ship noise in parts of the southern oceans. Here, we model underwater sound in the Australian Exclusive Economic Zone (EEZ) from ships and wind over a 6-month austral winter period, and validate the model with 6-month recordings from 25 stations. We chose the winter months as this is the peak of baleen whale presence (e.g., [34–36]). The aim is to enable a better understanding of where shipping noise is likely to be a significant contributor to the marine soundscape and thus, a potential stressor to marine life.

2. Materials and Methods

In a nutshell, we used ship tracks from Automatic Identification System (AIS) logs and underwater source spectra from the literature. On a 5 km × 5 km grid over the Australian EEZ, we modelled underwater sound propagation from all source cells (i.e., cells that contained ships) to all surrounding receiver cells over a 100 km radius. We then integrated sound exposure over the austral winter. The computational effort was managed by (1) splitting the EEZ into 28 acoustic zones, in which sound propagates in similar ways [37], hence, where a similar model may be set up, and (2) using a neural network to cluster all source-receiver transects within a zone into 64 groups of bathymetry transects, and modelling sound propagation only for cluster centroids. An overview of the process step-by-step is given in Appendix A. Wind noise was not propagated, but simply computed based on hourly wind speed data in each cell.

All GIS analysis was done with a combination of ArcMap (version 10.5, ESRI, Redlands, CA, USA) and R (Version 4.03, R Core Team, Vienna, Austria). Noise modelling and validation was done in MATLAB (Version 2020b, The MathWorks Inc., Natick, MA, USA). We commenced with a GIS layer of the Australian marine bathymetry, gridded to 5 km × 5 km [38].

2.1. Ship Data

Data on ship type, size, position, and speed were obtained from Automatic Identification System (AIS) logs managed by the Australian Maritime Safety Authority (AMSA). AIS data were extracted for the period 1 April 2015–30 September 2015. Ships were grouped

into five classes based on their length only (and not by type or function; e.g., tanker versus passenger ferry): <25 m, ≥25–<50 m, ≥50–<100 m, ≥100–<200 m, and ≥200 m. The regularity of the AIS location reporting depends on location and time, and the data we used was subsampled to provide locations, at most, every 5 min. From this data, ship tracks were interpolated by dead reckoning to intervals of 60 s if two successive AIS positions met criteria based on the time between the polls and the straightness of the vessel's path (as per Appendix B in [39]). For each ship track, the time spent in each grid cell was computed, and time was summed over all ships belonging to the same class, yielding a grid of cumulative time spent in each cell over the 6-month period, by ship class.

Underwater ship noise source spectra were taken from the Research Ambient Noise Directionality (RANDI) model [40] and integrated into full-octave bands: ≥10–<20 Hz, ≥20–<40 Hz, ≥40–<80 Hz, ≥80–<160 Hz, ≥160–<320 Hz, ≥320–<640 Hz, ≥640–<1280 Hz, and ≥1280–<2560 Hz (Figure 1a). The broadband (10 Hz–2.6 kHz) source levels were: 148, 160, 172, 187, and 193 dB re 1 µPa m, for the five classes, respectively.

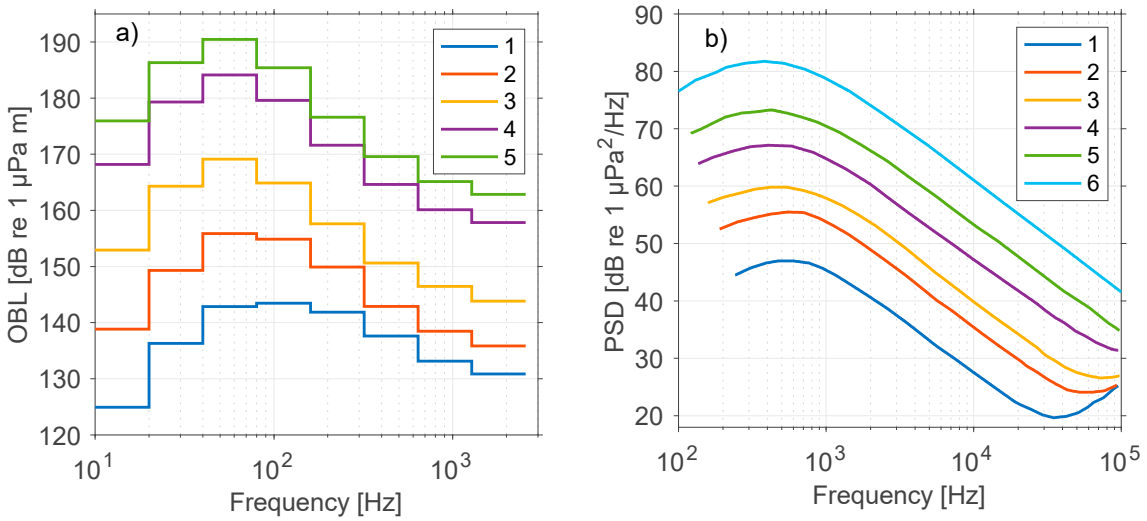

Figure 1. (**a**) Underwater ship noise source levels as full-octave band levels (OBL) for ships of lengths <25 m (Class 1), ≥25–<50 m (Class 2), ≥50–<100 m (Class 3), ≥100–<200 m (Class 4), and ≥200 m (Class 5); (**b**) Power spectral density levels (PSD) of wind noise under water at wind speeds 1–3 kn (Beaufort 1; curve 1), 4–6 kn (Beaufort 2; curve 2), 7–10 kn (Beaufort 3; curve 3), 11–21 kn (Beaufort 4–5; curve 4), 22–47 kn (Beaufort 6–9; curve 5), and ≥48 kn (≥Beaufort 10; curve 6).

2.2. Wind Data

Hourly data on surface wind speed (10 m altitude) were obtained over a similar 6-month period (1 April 2012–30 September 2012) from the Bureau of Meteorology and CSIRO [41], based on the NCEP Climate Forecast System [42]. The data varied in spatial resolution (4, 10, and 24 arcminute grids), which we projected and re-sampled to a 5 km × 5 km UTM grid. Over all grid cells, wind speed varied between 0.5 and 30 m/s (i.e., 1–58 kn). Wind speeds were binned to match the sea states represented in the 'Wenz curves' [43] and noise spectra were assigned to each wind speed bin (Figure 1b). The 'Wenz curves' were converted to linear power spectral density, then integrated over frequency, before applying $10\log_{10}$ to yield broadband mean-square sound pressure levels. Expressed as root-mean-square sound pressure levels, the associations became: 79 dB re 1 µPa for ≥1–<4 kn, 87 dB re 1 µPa for ≥4–<7 kn, 92 dB re 1 µPa for ≥7–<11 kn, 99 dB re 1 µPa for ≥11–<22 kn, 105 dB re 1 µPa for ≥22–<48 kn, and 113 dB re 1 µPa for ≥48 kn.

2.3. Acoustic Zones

The Australian EEZ had previously been broken up into 28 'acoustic zones' (Figure 2), whereby each zone was characterised by a unique set of hydroacoustic parameters of the water (i.e., sound speed profiles), geoacoustic parameters of the seafloor (i.e., thickness of

the sediment layer, density, compressional sound speed and attenuation, and shear sound speed and attenuation), and bathymetric parameters (i.e., water depth and slope) [37]. The idea was to set up one sound propagation environment for each zone and then model all of the ships in that zone.

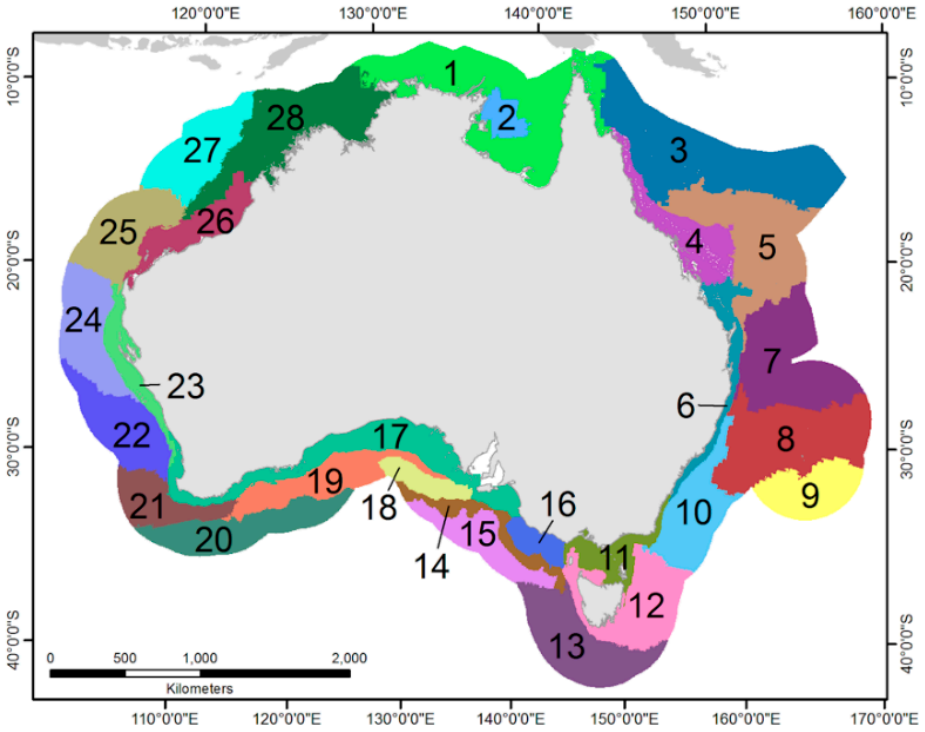

Figure 2. Map of the marine acoustic zones of the Australian EEZ [37].

2.4. Source-Receiver Transects

Within each zone, all of the grid cells that had a cumulative ship time > 0 (no matter the ship class) were identified. From each of these 'source cells', 36 radials were cast at 10-degree intervals. The bathymetry was extracted along each of these radials in 5 km steps out to a maximum range of 100 km, yielding thirty-six 100 km source-receiver transects around each source. A bathymetry reading at 2.6 km range from the centre of each source cell was added, representing the mean distance between two random points inside a square (i.e., 0.5214 times the edge length [44]). If a transect hit land, all subsequent bathymetry samples were set to 'not a number' along this 100 km transect. If a source sat near a zone boundary, then the 100 km transects were extracted with bathymetry from the neighbouring zone or from a 100 km buffer around the outside of the EEZ.

All of the transects from all of the source cells (of all ship classes) within a zone were passed to an unsupervised Kohonen neural network (i.e., a self-organizing map, SOM) with 900 neurons [45] (also see [13], where this SOM was previously used to cluster bathymetry transects). The neural net sorted the transects into 900 groups, based on their bathymetric shape. Further grouping was achieved by k-means clustering allowing for 64 clusters [46]. Cluster centroids were computed as the arithmetic mean of all transects within one cluster (see examples for Zone 16 in Figure 3). Sound propagation was modelled along each of the 64 centroids within one zone.

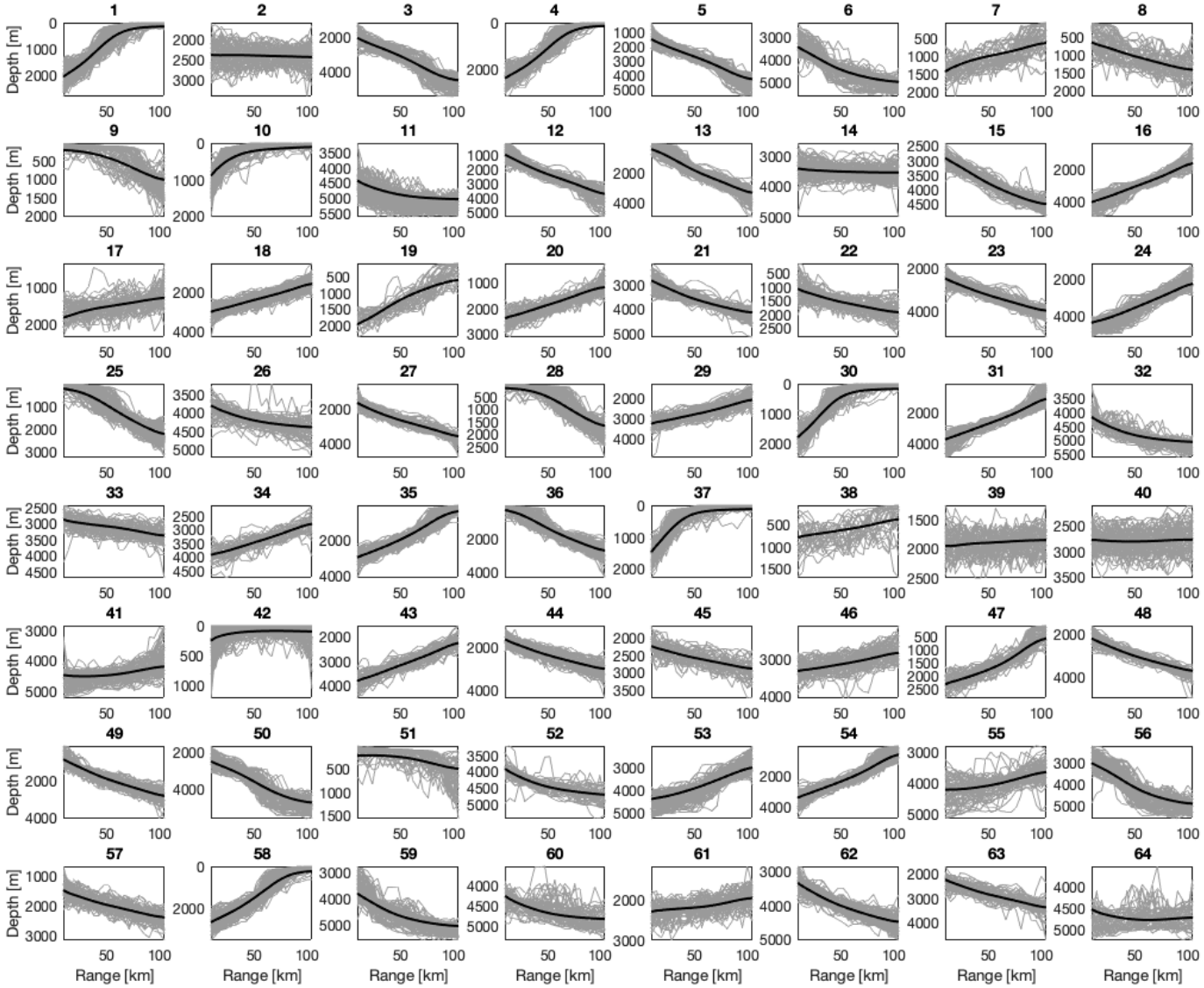

Figure 3. Graphs of all 98,532 source-receiver transects of Zone 16 plotted by cluster (grey), with centroid bathymetries shown in black. X-axes are range (km) and Y-axes are depth below the sea surface (m). Note the changing Y-ranges.

2.5. Sound Propagation Model

Sound propagation over each centroid bathymetry was modelled with RAMGeo in AcTUP V2.8 [47] (https://cmst.curtin.edu.au/products/underwater/ accessed on: 27 March 2021) based on zone-specific acoustic environments consisting of three layers: the water column, an unconsolidated surface sediment layer, and a consolidated calcarenite sediment layer as a half space. Water column parameters included the zone's mean sound speed profile [37] and water density profile. Representative temperature and salinity data were extracted from the World Ocean Atlas [48,49] to calculate water densities based on the UNESCO formula for sea water density [50]. Unconsolidated surface sediment layers throughout the EEZ comprised predominantly fine material (silt-sand) with sufficiently low shear wave speeds (<250 m/s) to allow modelling as a fluid. Hence, unconsolidated surface sediment parameters only included the zone-specific layer thickness, compressional sound speed, compressional wave attenuation, and density [37]. Surface sediment layer thickness was estimated as 0.5 m for zones within the sediment-starved carbonate platform [51]. Surface sediment thickness in the remaining zones appears variable [52–57], and so was modelled as 2 m.

In contrast to the surface sediment layer, calcarenite acts as an elastic material with a shear sound speed of 1400 m/s resulting in important propagation effects [51]. While RAMGeo is a parabolic equation for fluid seabeds, reasonable results can be obtained by using an equivalent fluid approximation with reflection coefficients representative of the elastic model [58]. The procedure to find an equivalent fluid approximation for each zone included (a) creating an environment with calcarenite as an elastic material (see [51] for geoacoustic properties), (b) creating an environment with calcarenite as a fluid layer starting with a compressional sound speed of 1250 m/s and a compressional wave attenuation of 4.5 dB/λ_c, (c) calculating the reflection coefficients for each modelled frequency for both environments with the reflection coefficient model BOUNCE [59], and (d) adjusting the fluid layer parameters until a representative equivalent had been reached (Figure 4).

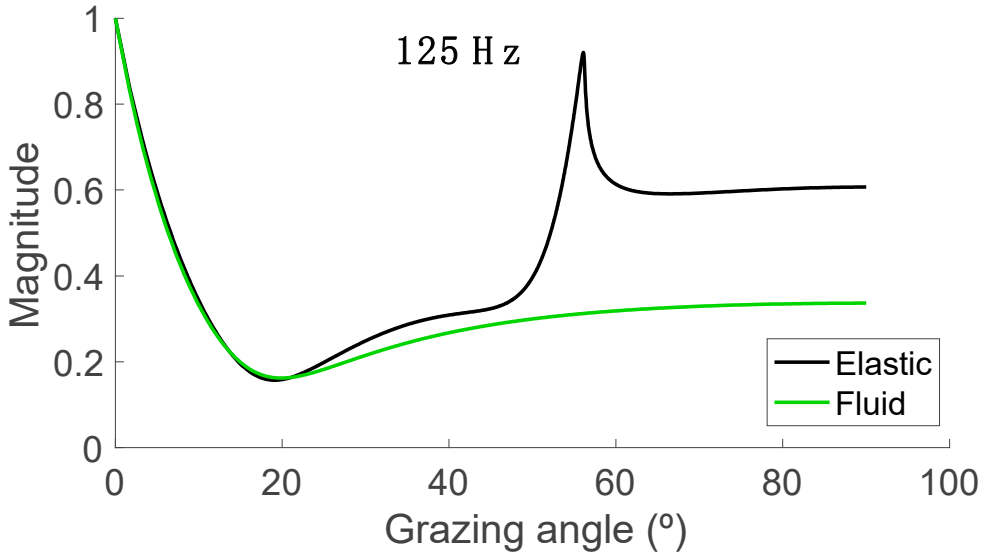

Figure 4. Example of the reflection coefficients of an elastic model (blue line) and a representative fluid model (green line) calculated with BOUNCE at 125 Hz.

RAMGeo modelled sound propagation loss for the centre frequencies of eight full-octave bands between 10 and 2000 Hz over a range of 100 km and up to 7100 m depth, which is more than the maximum water depth (6388 m) of the EEZ. The depth and range resolutions were 10 m. The source depth for all ships was chosen as 5 m below the sea surface. An example RAMGeo output at 640 Hz for the 64 centroid bathymetries of Zone 16 is shown in Figure 5. The bathymetry itself is just visible as a black line, below which propagation loss was greatest. The colours vary from 60 dB propagation loss (dark red) to 110 dB (dark blue). Several patterns are obvious: Convergence zones appeared over all deep bathymetries, leading to low propagation loss (i.e., high received levels) near the sea surface about 60 km from the source (i.e., clusters 6, 11, 26, 32, 41, 52, 53, 55, 59, 60, and 64). Over upwards-sloping bathymetries, propagation loss was greatest (e.g., clusters 1, 4, 19, 35, 37, 54, and 58). Over downwards-sloping bathymetries, sound may reflect into the deep-ocean sound channel, which has an axis at about 1 km depth off Australia. Once inside the channel, sound may propagate over vast ranges at very little additional loss because of no further seafloor (and to a lesser extent, sea surface) interactions (i.e., clusters 12, 13, 25, 36, and 49). Finally, RAMGeo does not include frequency-dependent absorption and so this additional loss was applied outside of and after RAMGeo [60].

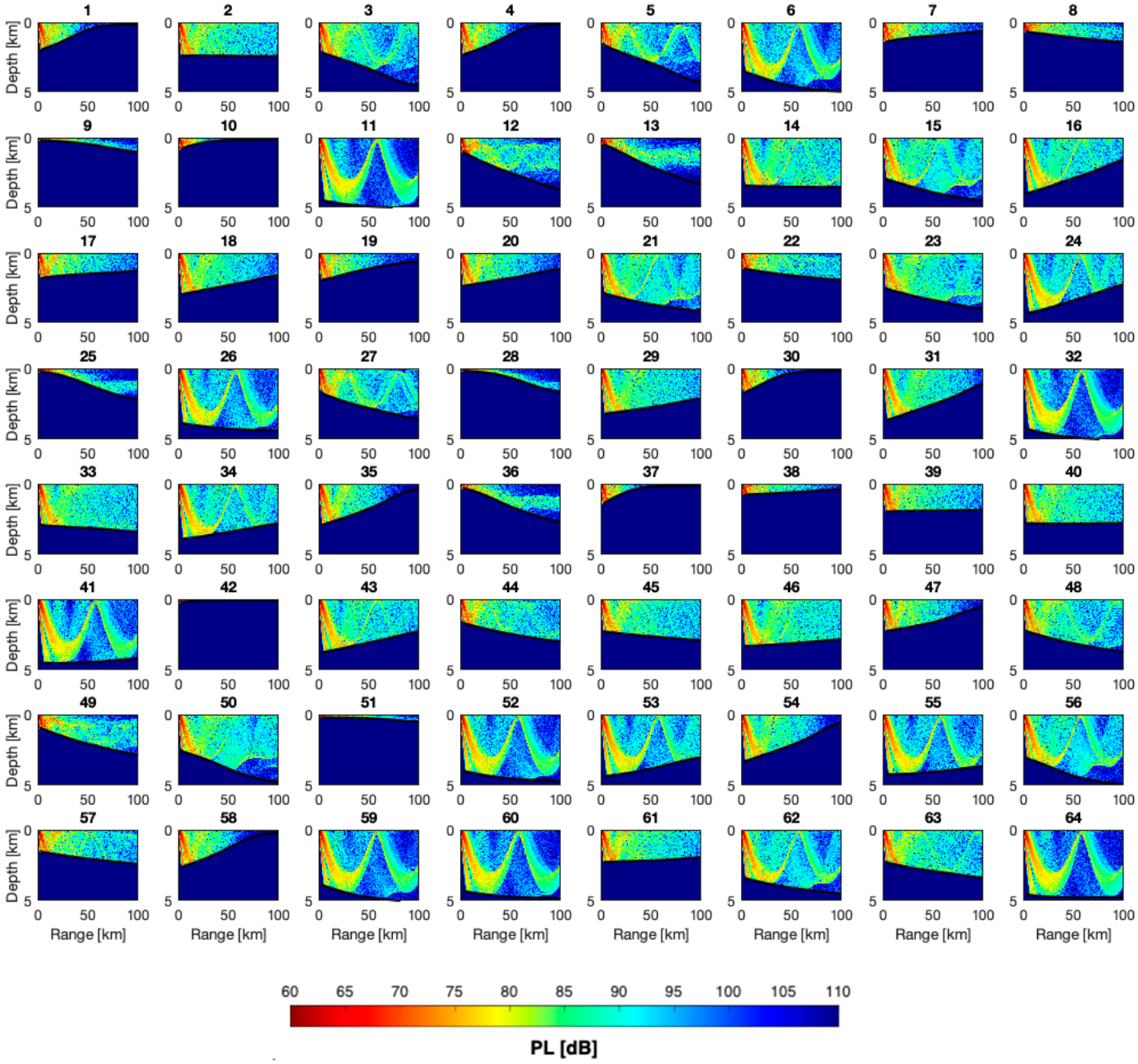

Figure 5. Plots of propagation loss (PL) as a function of range and depth along the 64 centroid bathymetries from Zone 16, for a frequency of 640 Hz. The darkest red corresponds to 60 dB and the darkest blue to 110 dB. X-axes are range (km) and Y-axes are depth below the sea surface (km); both are scaled linearly.

2.6. Accumulation of Received Levels

Within each zone, one ship class was treated at a time. The source cells corresponding to one ship class were found, thirty-six 100 km radials were cast at 10-degree intervals around each source cell, and bathymetry was extracted along each radial and sampled in 5 km steps; the mean distance between a ship and a receiver of 2.6 km within the source cell was inserted at the beginning. In other words, source cells were assigned a received level at 2.6 km. Then, stepping through the source cells for this ship class in this zone, for each of the 36 radial transects, the best matching centroid bathymetry was found. In fact, as the SOM had been trained with all source-receiver transects from all ship classes in this zone, finding the 'best matching centroid' reduced to simply looking up into which cluster this transect originally went. Then, for each frequency modelled, propagation loss (*PL*) along this centroid was recovered and subtracted from the corresponding octave band

source level (*SL*) plus the cumulative time in dB re 1 s (with *T* in units of second) of this ship class in this source cell, yielding received levels (*RL*):

$$RL = SL + 10\log_{10}(T) - PL$$

In this equation, *SL* is a number, the octave band source level expressed as a mean-square pressure level [dB re 1 μPa^2] at the modelled frequency. The duration term is also a number [dB re 1 s]. *PL* [dB], however, is a matrix with values in depth and range. Therefore, *RL* is a matrix containing received sound exposure levels (*SEL*) [dB re 1 $\mu Pa^2 s$] as a function of range and depth. There was one such *RL* matrix for each frequency.

To change from the polar coordinates (in which sound propagation was modelled) to the Cartesian grid of the EEZ, *RL* was interpolated to the 5 km grid of the EEZ, at each depth. Including frequency as an additional dimension, this yielded a 4-dimensional matrix of longitude, latitude, depth, and frequency, covering the entire EEZ. The matrix was populated cumulatively by summing sound exposure (i.e., in linear, not logarithmic terms) over all 36 transects about each source cell, and then over all source cells, before taking 10 $\log_{10}$ again to yield cumulative sound exposure levels (*C-SEL*).

2.7. Ship Noise Map

Broadband sound exposure levels were computed by summing sound exposure over frequency, thereby reducing the matrix to three dimensions, then converting to dB. A further reduction to two dimensions was achieved by finding the maximum sound exposure level over the top 200 m, representing the 'worst case' of exposure for animals that dive over this depth [61]. One such map is presented for each ship class, as well as cumulatively over all five classes. These maps of cumulative sound exposure level were accumulated over six months encompassing the austral winter. They can be read as average mean-square sound pressure level (*SPL*) maps by subtracting the 6-month duration in dB re 1 s:

$$SPL = C\text{-}SEL - 10\log_{10}(183\ \text{d} \times 24\ \text{h/d} \times 60\ \text{min/h} \times 60\ \text{s/min/s}) = C\text{-}SEL - 72\ \text{dB re 1 s}$$

2.8. Wind Map

The wind map was produced by converting the hourly root-mean square sound pressure levels to linear mean-square sound pressures, then integrating over time, and converting back to decibel. 10 $\log_{10}(3600)$ was added to account for the number of seconds per hour, yielding cumulative sound exposure levels from wind at each cell over the 6-month winter period.

2.9. Comparison between Ship and Wind Noise

For comparison, the cumulative sound exposure levels from wind were subtracted from those of ships (summed over all classes) in every grid cell, and plotted, to show in which geographic regions one dominated over the other. We also added the modelled sound exposures from ships and wind, then converted to decibel, to plot the combined ambient noise exposure levels over the 6-month period.

2.10. Validation

Archival underwater acoustic recordings from the northwest, west, south, and south-east of Australia were used in an attempt to validate the modelled noise maps. These data were collected by autonomous recorders [62] deployed over winter between 2006 and 2017. All recorders had been moored on the seafloor, and sampled at 6 kHz, 5 min every 15 min. Most of these datasets were collected while the passive acoustic observatories of Australia's Integrated Marine Observing System (IMOS) were operational and are thus available from the Australian Ocean Data Network (AODN) (https://acoustic.aodn.org.au/acoustic/ accessed on: 15 March 2021).

Long-term spectral averages (LTSA) were computed in 5 min windows and integrated over frequency (10–2000 Hz) and time (1 April–30 September) to yield cumulative sound

exposure. LTSAs were visualised in the software CHORUS [63] to provide an overview of the soundscape and its contributors over multiple weeks to months at a time. Spectrograms with a resolution of 1 s (50% overlap) were computed to zoom into any 5 min sample when the sound sources were not immediately identifiable in the LTSAs. Power spectral density percentile plots (in which the nth percentile gives the power spectral density level exceeded n% of the time, at each frequency) helped identify the dominant contributors to the winter soundscapes [64].

3. Results

Australia-wide maps of ship noise C-SEL (by class) over the period 1 April 2015–30 September 2015 are shown in Figure 6. Cumulative sound exposure levels over all classes are also plotted. Wind noise C-SEL, the level difference between ship noise C-SEL and wind noise C-SEL, and the combined C-SEL of ship and wind noise are shown in Figure 7. Hyperlinks to the data can be found in the Data Availability section.

Validation

Modelled C-SELs of ship and wind noise are compared to measured C-SELs from the validation datasets in Table 1. There is good agreement (to within 3 dB) between model and measurement noise levels at sites 9 (NW Shelf, WA, Australia), 16 (Bremer Canyon, WA, Australia), and 25 (Tuncurry, NSW, Australia). The former two were dominated by strong wind, the latter by ships. Figure 8A shows almost continuous strong wind at the Bremer Canyon site, a faint Antarctic blue whale (*Balaenoptera musculus intermedia*) chorus throughout winter, peaking in May, and distant passes of ships. The cumulative energy from wind dominates and is the reason for the good agreement between model and measurement. Figure 8B shows briefer periods of strong wind off Tuncurry and a distant Antarctic blue whale chorus. The dominant feature of this soundscape were numerous passes of ships at close range, and this is the reason for the good agreement between model and measurement at this site.

Disagreement between model and measurement noise levels at other sites was due to unaccounted, additional, non-targeted noise contributions to the soundscape: marine animals and industrial operations. Figure 9 provides an overview of the biological contributors to the soundscape. The stereotypical sounds of Omura's whales (*Balaenoptera omurai*); Antarctic blue whales; pygmy blue whales (*Balaenoptera musculus brevicauda*); the unidentified source of the spot call, fin whales (*Balaenoptera physalus*); dwarf minke whales (*Balaenoptera acutorostrata*), and humpback whales (*Megaptera novaeangliae*) have been well described in the literature; as have Australian fish choruses [65–67]. These animals dominated the winter soundscapes near islands and reefs (sites 1, 4, 6, 9, 12, 14, 15, 17 and 18). Examples of soundscapes almost free from ships but noisy with animals are shown in Figures 10 and 11. Examples of soundscapes affected by anthropogenic noise are shown in Figure 12. At the time of recording, seismic surveying was the most common anthropogenic source that we did not model.

We were able to determine C-SEL variability over time at nearby sites. Winter recordings at sites 17 (2016) and 18 (2017) differed in C-SEL by 1 dB; these sites were only 80 m apart. Similarly, sites 7 (2006) and 8 (2010) were 4 km apart and the C-SEL differed by 1 dB. Moreover, sites 14 (2014) and 15 (2016) were 4 km apart and the C-SEL differed by 1 dB, showing good consistency over 1–4 years at nearby sites. Sites 19–24 were all within 3 km of each other. Recordings were from 2012, 2014, 2015, 2015, 2016, and 2017, respectively. The two simultaneous sets differed by 1 dB in measured C-SEL. The 2014 set had the lowest C-SEL with 179 dB re 1 μPa^2s, and one of the 2015 sets had the highest C-SEL at 185 dB re 1 μPa^2s, indicating the level of variability that may be expected from such in situ recordings over multiple years. There was no linear trend.

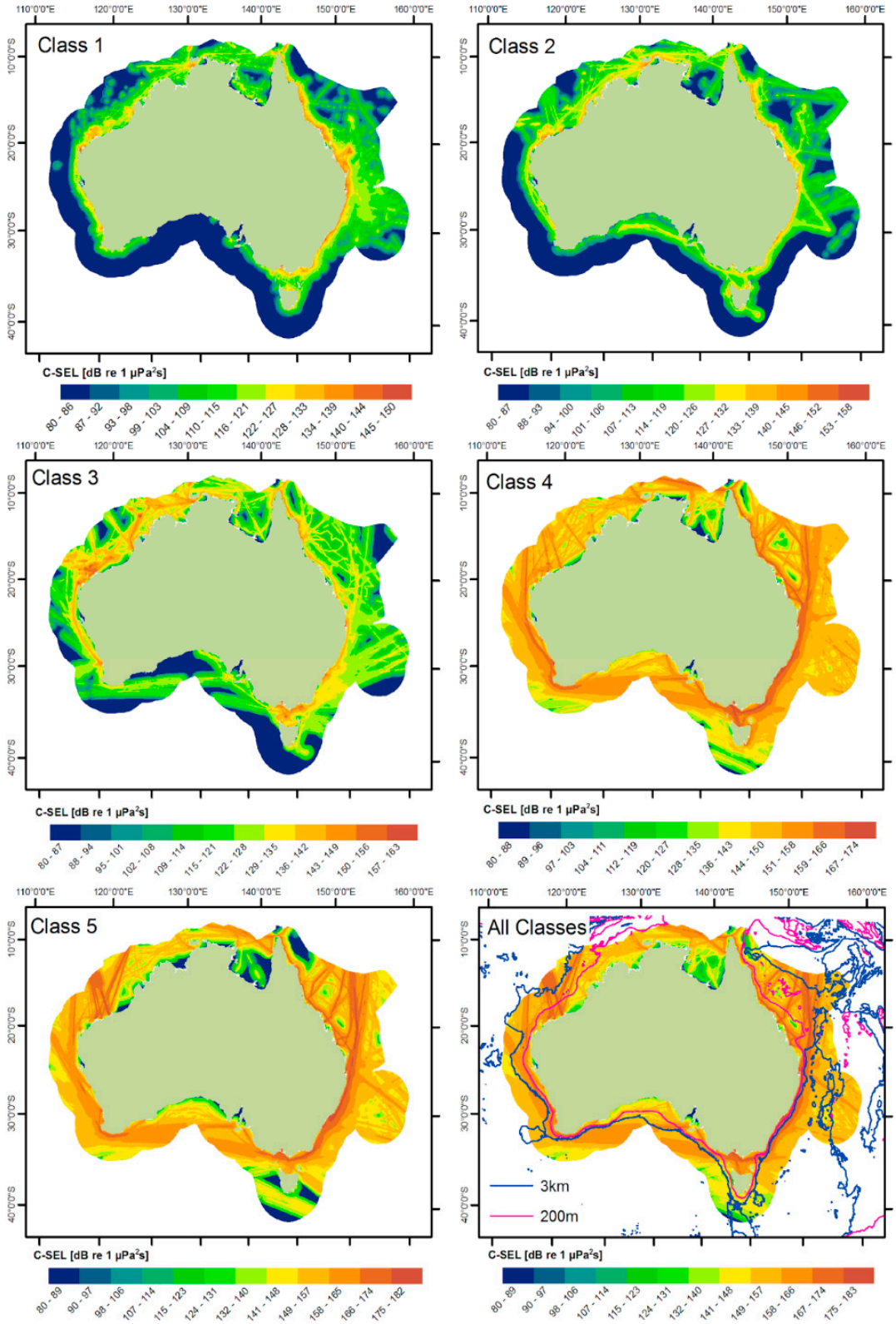

Figure 6. Maps of cumulative sound exposure levels (C-SEL) from shipping in the Australian EEZ, by ship class, and cumulatively over all classes. Maximum received C-SEL over the top 200 m of water were picked, representing a 'worst case' for animals that dive within this depth. Sound exposure was accumulated over 183 days (1 April 2015–30 September 2015). Levels can be converted to average mean-square sound pressure levels by subtracting 72 dB re 1 s. Note that the colour bars all start at 80 dB but the highest levels differ, reflective of the peak C-SEL for each class. The final map also shows 200 m and 3 km bathymetry contours.

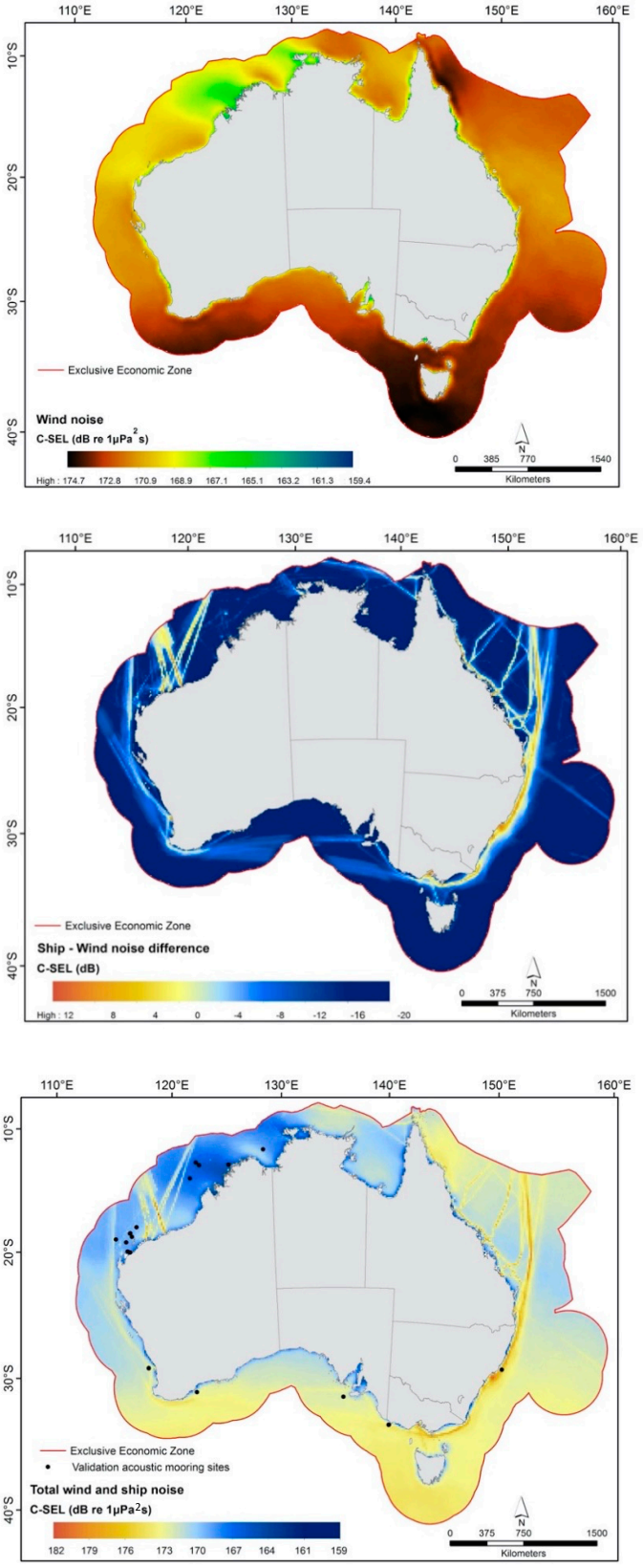

Figure 7. Maps of modelled wind noise within Australia's EEZ during winter 2012 (1 April–30 September: **top**), ship C-SEL less wind C-SEL (**middle**), and C-SEL from ships and wind combined (**bottom**). The black dots identify underwater recording stations used for validation. To convert to mean sound pressure level, subtract 72 dB re 1 s.

Table 1. Site ID, location, year, measured C-SEL and SPL, modelled C-SEL from ships, wind, and combined, C-SEL difference between model and measurement, and rough description of the soundscape.

ID	Location	Longitude	Latitude	Winter	C-SEL [dB re 1 μPa^{2}s] Measured	SPL [dB re 1 μPa] Measured	Ship C-SEL [dB re 1 μPa^{2}s] Modelled	Wind C-SEL [dB re 1 μPa^{2}s] Modelled	Ship + Wind C-SEL [dB re 1 μPa^{2}s] Modelled	C-SEL Difference Measured-Modelled [dB]	Notes
1	Bonaparte Gulf WA	128.2	−13.1	2012	174	102	144	170	170	4	dominated by Omura′s whale chorus throughout winter; some fish choruses; strong wind periods; some ships; distant seismic survey
2	NW Shelf	121.9	−14.1	2008	192	120	140	167	167	25	dominated by industrial noise at the time
3	NW Shelf	122.2	−14.3	2008	184	112	154	167	167	17	dominated by 3 seismic surveys at different ranges covering entire winter
4	NW Shelf	124.9	−14.4	2007	176	104	148	166	166	10	dominated by fish choruses, very little anthropophony; pristine
5	NW Shelf	121.3	−15.5	2013	172	100	151	168	168	4	3 seismic surveys overlapping in time at different ranges; Omura′s whales and humpback whales

Table 1. *Cont.*

ID	Location	Longitude	Latitude	Winter	C-SEL [dB re 1 μPa^{2}s] Measured	SPL [dB re 1 μPa] Measured	Ship C-SEL [dB re 1 μPa^{2}s] Modelled	Wind C-SEL [dB re 1 μPa^{2}s] Modelled	Ship + Wind C-SEL [dB re 1 μPa^{2}s] Modelled	C-SEL Difference Measured-Modelled [dB]	Notes
6	NW Shelf	115.9	−19.4	2013	177	105	155	170	170	7	strong humpback whale song
7	NW Shelf	115.2	−19.9	2006	183	111	157	170	170	13	dominated by seismic surveys all winter
8	NW Shelf	115.3	−19.9	2010	184	112	160	170	170	14	strong industrial noise throughout
9	NW Shelf	115.4	−20.2	2010	172	100	160	170	170	2	several strong fish choruses and periods of strong wind; pristine
10	NW Shelf	113.9	−20.2	2012	184	112	155	169	170	14	a lot of industrial noise and seismic survey
11	NW Shelf	114.8	−20.6	2010	186	114	153	169	170	16	dominated by industrial noise and seismic surveys, near and far
12	NW Shelf	114.8	−21.4	2010	180	108	157	169	169	11	dominated by humpback whale and fish choruses, also dwarf minke chorus; pristine
13	NW Shelf	115.0	−21.5	2010	177	105	157	168	168	9	industrial noise, fish choruses throughout, humpback whales from 1 Aug.

Table 1. *Cont.*

ID	Location	Longitude	Latitude	Winter	C-SEL [dB re 1 μPa^{2}s] Measured	SPL [dB re 1 μPa] Measured	Ship C-SEL [dB re 1 μPa^{2}s] Modelled	Wind C-SEL [dB re 1 μPa^{2}s] Modelled	Ship + Wind C-SEL [dB re 1 μPa^{2}s] Modelled	C-SEL Difference Measured-Modelled [dB]	Notes
14	Perth Can yon WA	115.0	−31.8	2014	180	108	164	172	172	8	dominated by pygmy blue whale chorus, also strong fish chorus throughout; fin whales in June; spot call in June–July; humpback whales in Sept.
15	Perth Can yon WA	115.0	−31.9	2016	179	107	164	172	172	7	dominated by pygmy blue whale chorus, also strong fish chorus throughout; fin whales in June; spot call in June–July; humpback whales in Sept.
16	Bremer Canyon WA	119.6	−34.7	2015	175	103	158	172	172	3	quiet soundscape with blue whale and spot call chorus and wind; distant shipping only noticeable <5% of the time

Table 1. *Cont.*

ID	Location	Longitude	Latitude	Winter	C-SEL [dB re 1 μPa^{2}s] Measured	SPL [dB re 1 μPa] Measured	Ship C-SEL [dB re 1 μPa^{2}s] Modelled	Wind C-SEL [dB re 1 μPa^{2}s] Modelled	Ship + Wind C-SEL [dB re 1 μPa^{2}s] Modelled	C-SEL Difference Measured-Modelled [dB]	Notes
17	Kangaroo Isl. SA	135.9	−36.1	2016	180	108	156	173	173	7	dominated by Antarctic blue whale chorus; spot calls; fish; strong wind; very few ships
18	Kangaroo Isl. SA	135.9	−36.1	2017	179	107	156	173	173	6	dominated by choruses of Antarctic blue whales, pygmy blue whales, spot calls, and fish
19	Portland VIC	141.2	−38.5	2012	181	109	167	173	174	7	strong wind and ships; Antarctic blue whale chorus entire winter; strong spot call in Aug.
20	Portland VIC	141.2	−38.5	2014	179	107	167	173	174	5	3 overlapping whale choruses (Antarctic blue, pygmy blue, spot call); wind and ships
21	Portland VIC	141.2	−38.5	2015	184	112	167	173	174	10	strong wind; strong fish; Antarctic blue whale chorus for nearly entire winter in the ship noise band; spot call in July–Aug.

Table 1. *Cont.*

ID	Location	Longitude	Latitude	Winter	C-SEL [dB re 1 μPa^{2}s] Measured	SPL [dB re 1 μPa] Measured	Ship C-SEL [dB re 1 μPa^{2}s] Modelled	Wind C-SEL [dB re 1 μPa^{2}s] Modelled	Ship + Wind C-SEL [dB re 1 μPa^{2}s] Modelled	C-SEL Difference Measured-Modelled [dB]	Notes
22	Portland VIC	141.2	−38.5	2015	185	113	167	173	174	11	Antarctic blue whale chorus entire winter; spot call; strong fish; strong wind and ships
23	Portland VIC	141.2	−38.5	2016	180	108	167	173	174	6	broad ship noise hump at 50 Hz; choruses of Antarctic blue whale; pygmy blue whale; spot call, and fish
24	Portland VIC	141.2	−38.5	2017	181	109	167	173	174	7	Antarctic blue whale chorus and fish all winter; some strong pygmy blue whales; many ships
25	Tuncurry NSW	152.9	−32.3	2016	181	109	177	172	178	3	full of ships; blue whale choruses in the background

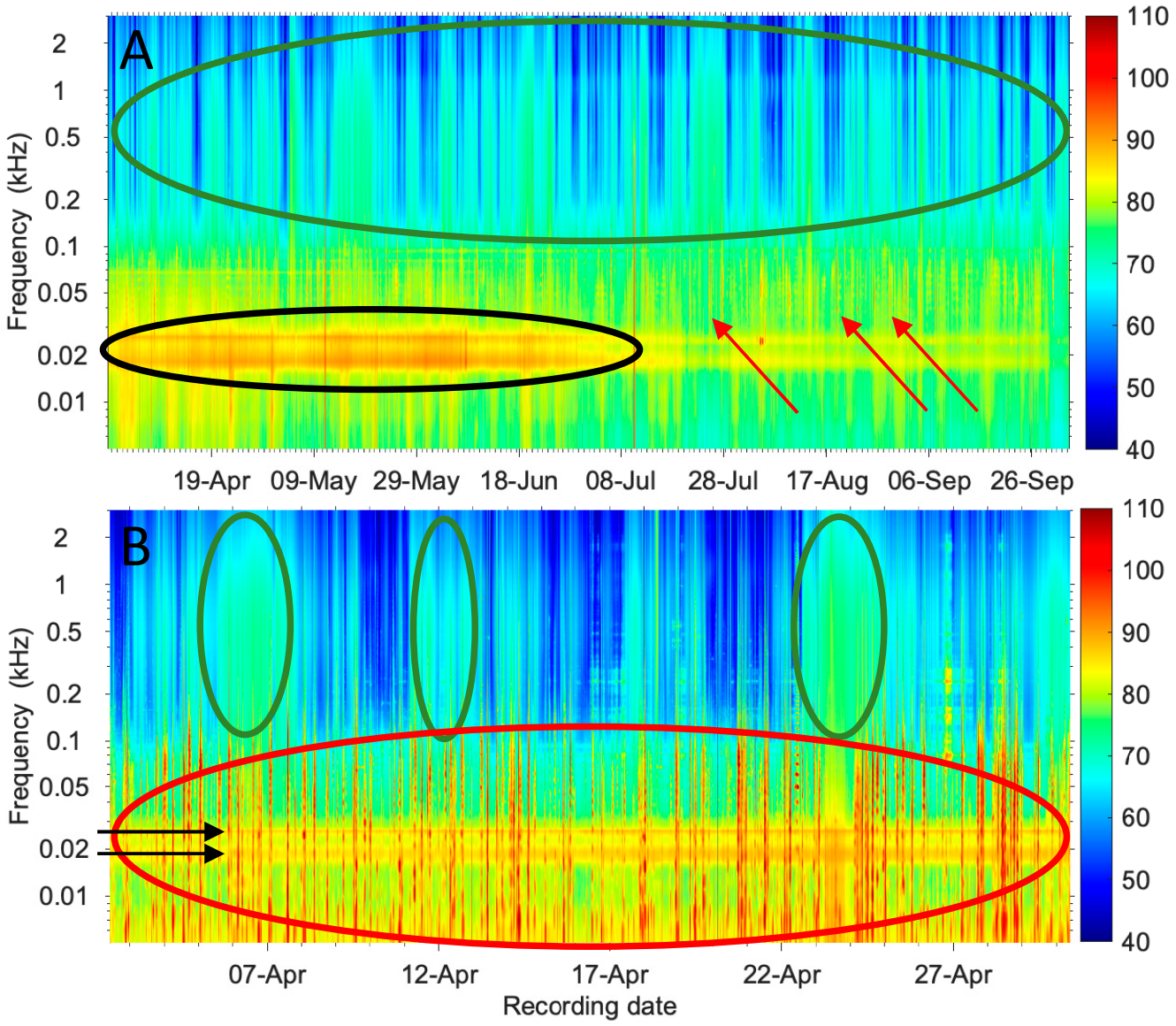

Figure 8. LTSAs [dB re 1 μPa^2/Hz] near (**A**) the Bremer Canyon, WA, site 16, and (**B**) Tuncurry, NSW, site 25. The contributions from ships, wind, and Antarctic blue whales (*Balaenoptera musculus intermedia*) are marked in red, green, and black, respectively. Only a few ships are marked in (**A**).

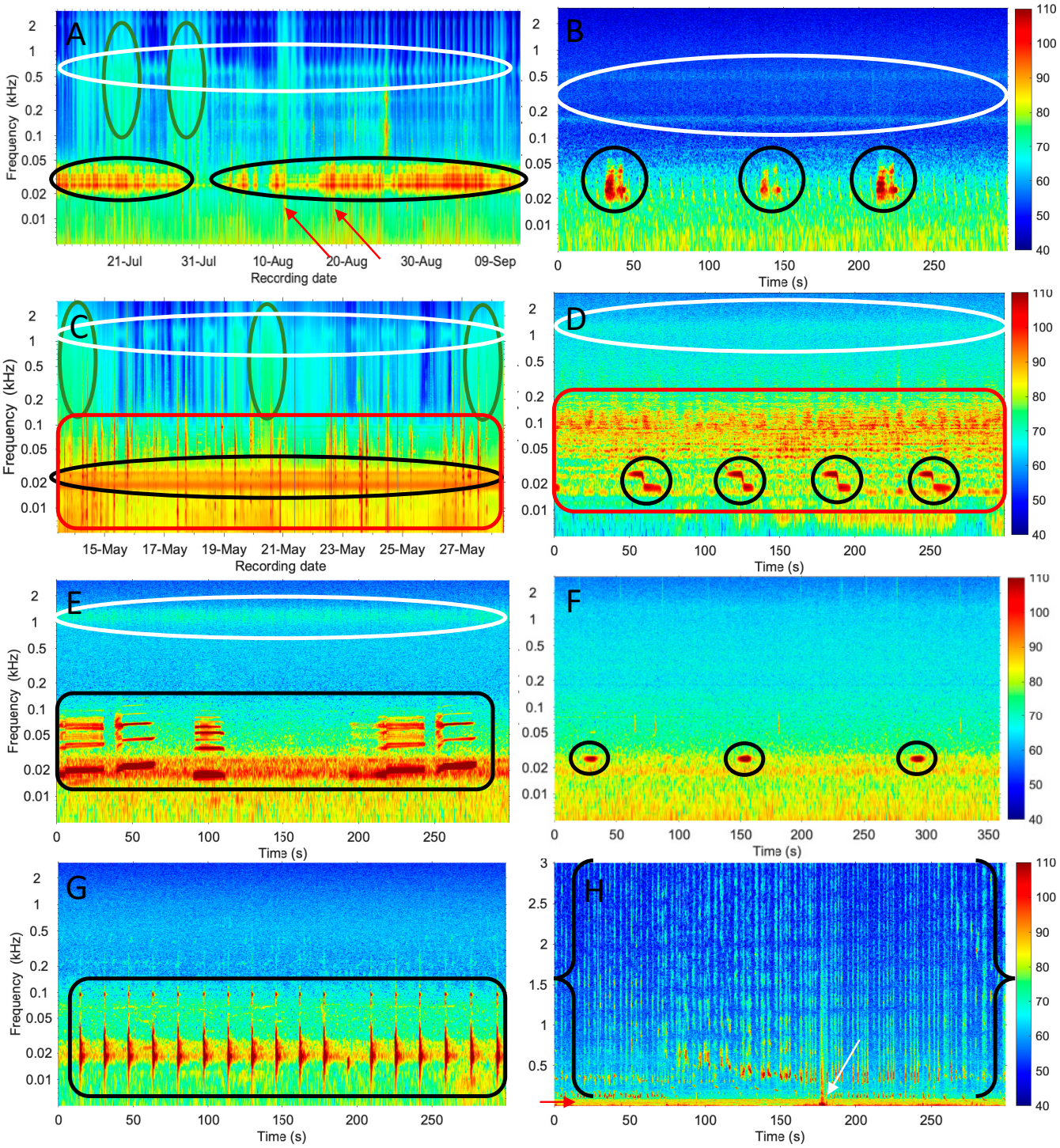

Figure 9. LTSAs and spectrograms [dB re 1 μPa^2/Hz] showing (**A**) an Omura's whale chorus and evening fish chorus at site 1; (**B**) Three Omura's whale calls and a fish chorus at site 5 (this specific example is free from ships and wind); (**C**) An Antarctic blue whale chorus and evening fish chorus at site 22; (**D**) Four Antarctic blue whale Z-calls and a fish chorus at site 23; (**E**) Pygmy blue whale song in front of the Antarctic blue whale chorus and a fish chorus at site 24; (**F**) Three spot calls at site 19; (**G**) Fin whale song at site 14; and (**H**) Humpback whale song at site 6. Note the changing x- and y-scales. All panels but H use a logarithmic y-scale. H uses a linear y-scale to stress the great bandwidth of humpback whale song (100 Hz–>3 kHz) in comparison to the narrow bandwidth of ship noise in this example (<100 Hz), resulting in humpback whales dominating the C-SEL after integration over frequency. An animal (fish?) biting on the hydrophone is marked by the white arrow. Sound from whales, fish, ships, and wind are marked in black, white, red, and green, respectively.

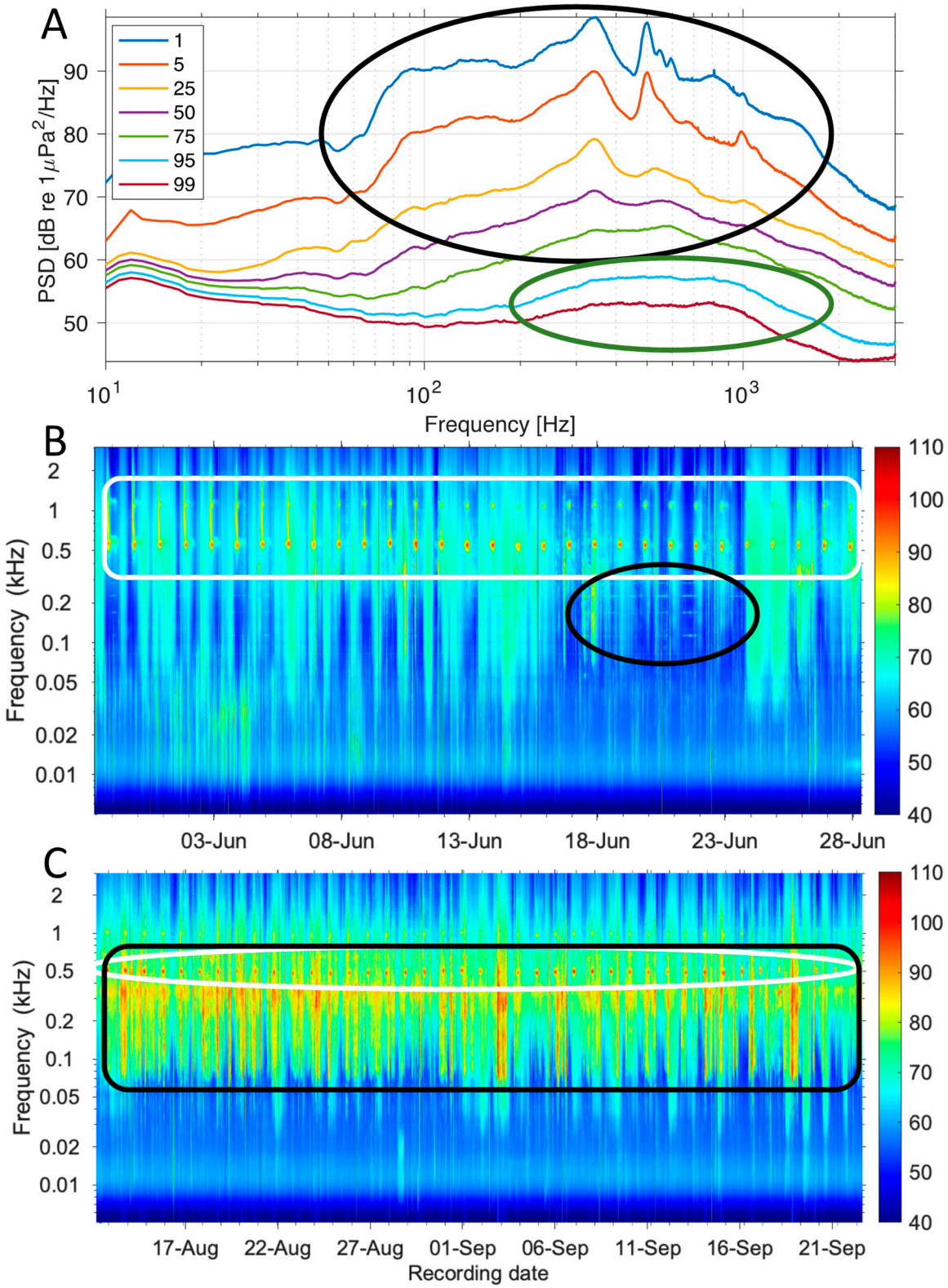

Figure 10. Winter soundscape at site 12. (**A**) Power spectral density percentiles showing domination by humpback whales from late June and fishes throughout. The curves follow the shape of the biological spectra 75% of the time (within black ellipse). The characteristic shape of wind is only seen in the absence of whales (lowest two percentiles within green ellipse); (**B**) LTSA of an evening fish chorus (within white box). A distant dwarf minke whale chorus (thin horizontal lines inside black ellipse) occurred in June–July. (**C**) LTSA showing humpback whales (within black box) and fish (within white ellipse).

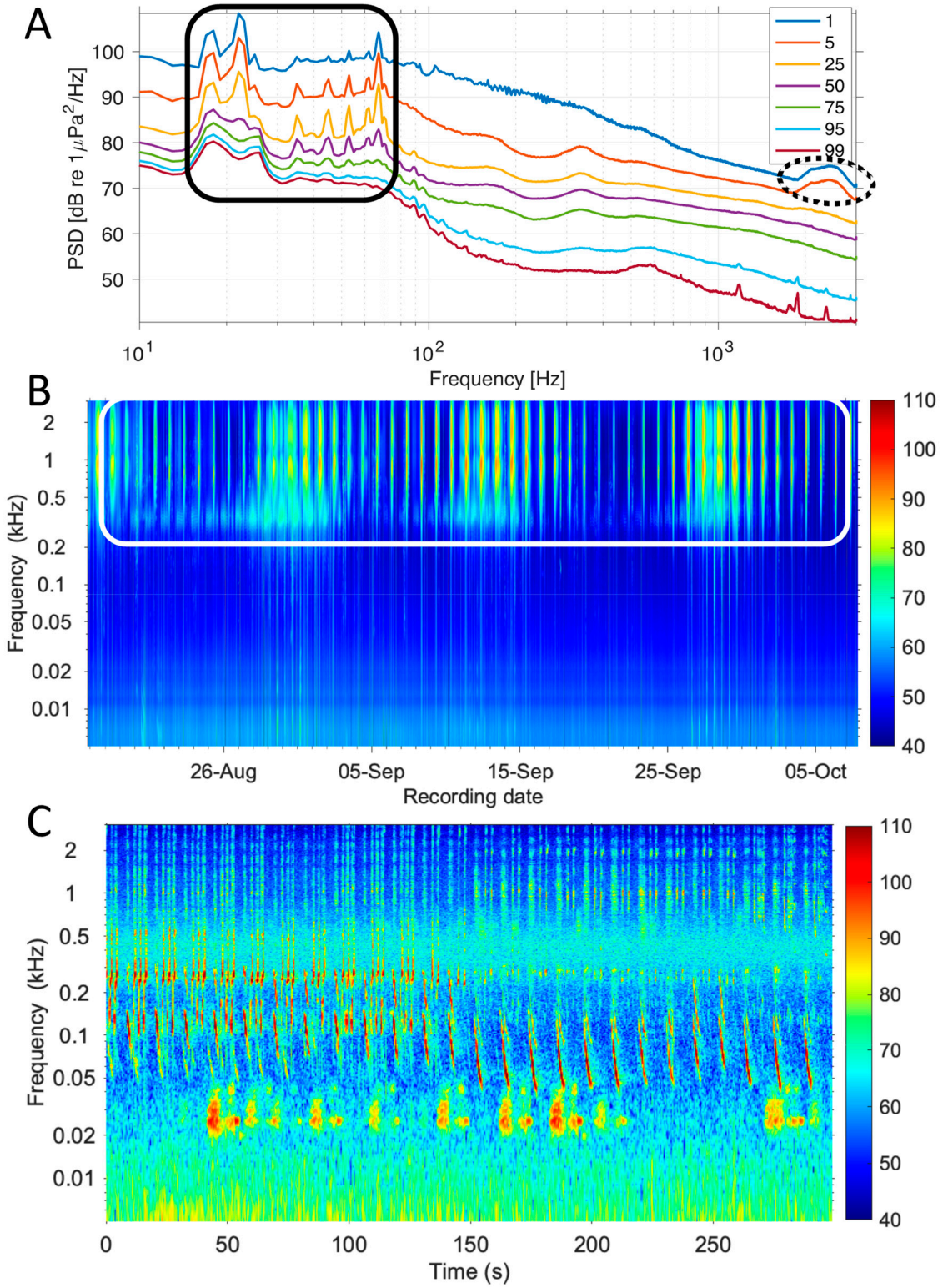

Figure 11. (**A**) Power spectral density percentiles of the winter soundscape at site 15 dominated by pygmy blue whales (within black box). The characteristic spectral shape of a fish chorus is seen at 2–3 kHz in the 1st and 5th percentiles (dotted); (**B**) LTSA of the pristine soundscape at site 4 exhibiting multiple fish choruses at night (within white box), whose intensities vary with the phase of the moon; (**C**) Spectrogram of the soundscape at site 1 showing at least two simultaneous whale species (Omura's whales at 20–50 Hz and one other at 50–3000 Hz, uncertain) and a fish chorus at 300–500 Hz.

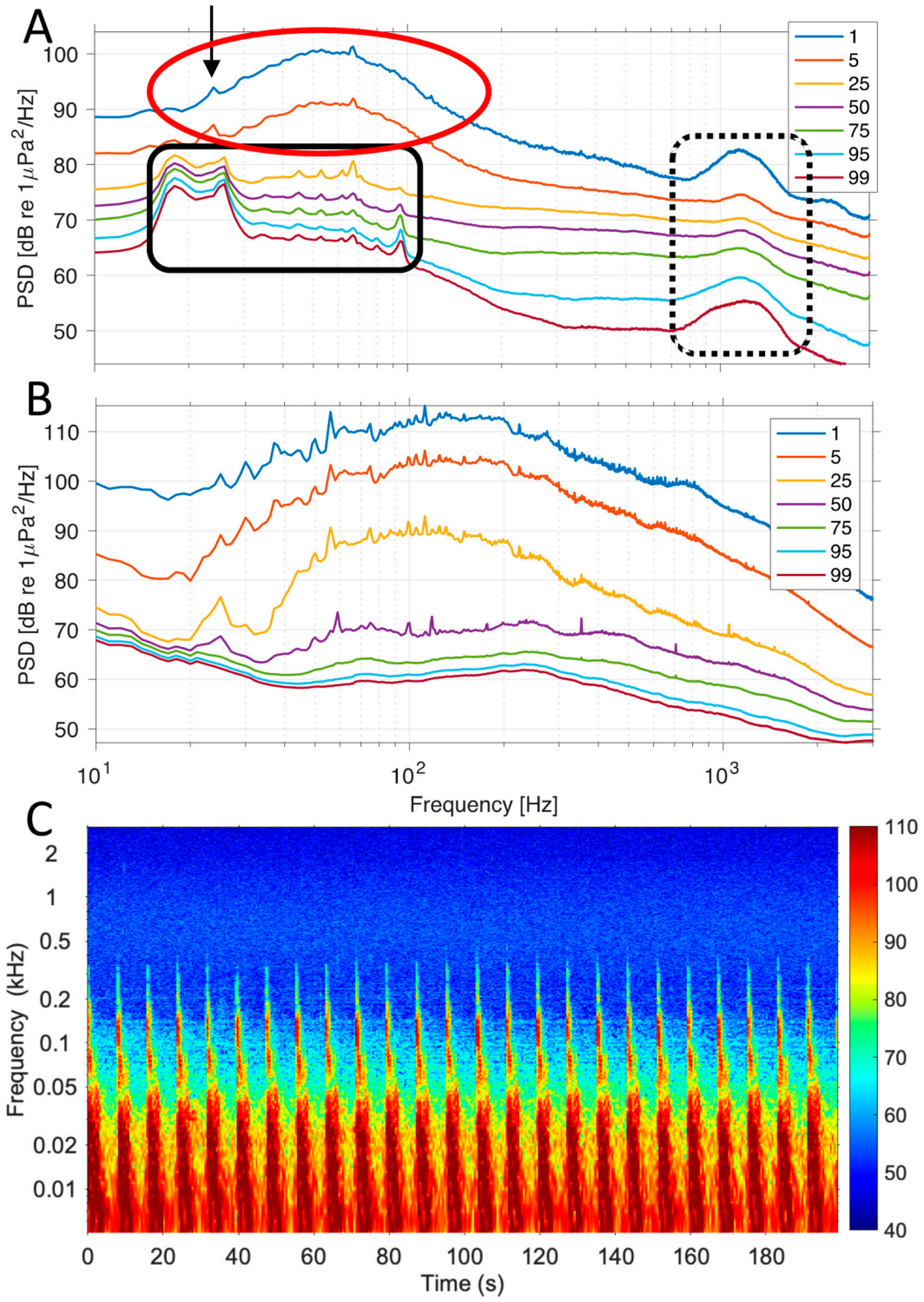

Figure 12. (**A**) Power spectral density percentiles of the winter soundscape at site 23 showing that pygmy blue whales (black box) were present the entire 6 months (because the spectral shape of their song is seen even in the 99th percentile, meaning it did not become quieter than this). However, the strongest sound in this soundscape came from ships (identified by the broad and smooth spectral hump between 20 Hz and 200 Hz; red ellipse). The spot call was also strong at this site (marked by the black arrow). The fish chorus at 800–2000 Hz (dotted box) was present the entire time as well; (**B**) Power spectral density percentiles from site 2 being entirely dominated by broadband industrial noise of unknown origin at this time; (**C**) Spectrogram of a strong seismic survey temporarily present at site 3; no other sounds were visible.

4. Discussion

The aim of our project was to develop a model for underwater ship noise in the Australian EEZ that could be used by industry and government to manage marine zones, their usage, stressors, and potential impacts. To put ship noise into context, we also modelled natural noise from wind under water. The models are based on numerous assumptions and involve a lot of averaging in space and time, leading to uncertainty. We therefore validated the models as a whole by comparing modelled sound exposure levels to measured underwater sound levels from 25 acoustic data sets collected over a 12-year span. Agreement was good when the underwater soundscape mostly contained the two sources modelled: ships and wind. Agreement was poorer when sound sources were missed (i.e., not modelled): seismic surveying, whales, and fishes.

Ship presence and movement were based on AIS data from the winter of 2015. Ships logged their positions at irregular time intervals, requiring that we interpolate between successive logs. We applied criteria for speed and direction continuity before straight-line interpolation, and where these were not met, we accepted holes in tracks, leading to an underestimation of ship time in the corresponding cells. We further had very few vessels in the smallest class (<25 m), as these mostly private recreational vessels do not log AIS positions. We therefore clearly underestimated their underwater noise contribution, in particular to coastal soundscapes. In addition, we did not take into account ships just outside of the EEZ and so underestimated noise levels near the EEZ boundary. Given that most AIS data were available for the larger and noisier vessels, we chose a monopole source depth corresponding to larger vessels (5 m) and applied this to all vessels in the model, for simplicity. The introduced uncertainty in modelled received levels is perhaps greater in winter (which we modelled) than summer, given all of our sound speed profiles exhibited a shallow surface duct of variable depth. Accounting for different source depths for the different vessel classes would require modelling sound propagation over the 64 cluster centroids in each zone multiple times, which we did not do, but could be done to improve accuracy. This might be desirable for more localised applications and modelling over smaller areas than the entire EEZ (e.g., regional seismic surveys or coastal developments). Placing the monopole at deeper depth than the propeller depth of small vessels during sound propagation modelling will likely enhance long-range received levels of the smaller, hence quieter, vessels, which are possibly underrepresented in the AIS data, meaning the errors do not add but work in reverse. Finally, the source levels produced by the RANDI model fall within the broadband quartiles reported recently [68]; however, the spectral shapes might differ. MacGillivray and de Jong [69] very recently showed that the RANDI model overpredicted source power spectral density below ~250 Hz for bulk carriers, vehicle carriers, tankers, container ships, and cruise ships, yet underpredicted source power spectral density above ~250 Hz. This might lead to differential errors in different regions (deep versus shallow water), depending on the efficiency with which sound below and above 250 Hz propagates in each environment. Other studies reported RANDI to overestimate [70,71] or underestimate, particularly above 200 Hz [72]. Underprediction of source levels by the RANDI model might be more common for the smallest vessels, in particular those with powerful motors, such as whale-watching boats and tugs [69,73–76].

In terms of the underwater sound propagation model used, the most common source of uncertainty is a lack of data on the seafloor composition and thus, acoustic properties. We used typical values from [51], but geoacoustic properties may vary from place to place. Hydroacoustic data (i.e., temperature, salinity, and sound speed profiles) were missing in some coastal zones and thus required spatial extrapolation. The equivalent fluid model applied is only approximate up to grazing angles of 50° and thus, more accurate for long-range propagation modelling. Modelling sound propagation only along bathymetry cluster centroids, instead of every source-receiver transect, introduced additional uncertainty. However, with a median water depth of 1809 m for all source cells in the entire EEZ, deviations of individual bathymetries from centroid bathymetries are likely to affect modelled received levels more in shallow and coastal rather than offshore waters. While

deviations in bathymetry from cluster centroids may change the pattern of constructive and destructive interference and thus yield rather variable received levels at specific locations in space and depth, there will not be a consistent bias in modelled received levels. Modelling along centroids will lead to both over- and underprediction, depending on range, depth, and frequency. These effects will be important on a fine spatial scale, but disappear on a coarse grid. Finally, the received level depends greatly on receiver depth. We chose to plot maximum received levels over the top 200 m, corresponding to the water layer in which most baleen whales travel. Any receiver depth (or depth range) may, of course, be picked from the model results, corresponding to specific animal depths.

The wind model we used was based on the classic review done by Wenz [43]. Other models, such as the Cato model [77] extend to lower frequencies and thus, yield higher levels (up to 2 dB) in high sea states. The Cato model would reduce the model-versus-measurement difference (i.e., improve the wind noise prediction) at the wind-dominated sites (9, 16).

The map of underwater ship noise was based on AIS data from the year 2015, the map of underwater wind noise was based on wind data from 2012, and the in situ measurements were from various years (2006–2017). For a fine-scale model (i.e., small grid size), the exact positions and types of vessels would matter and therefore, validation with measurements from different years might be less successful. However, on a coarse grid, fine-scale variability averages out. For the ship noise map to differ by 3 dB, twice the number of ships (i.e., twice the power) would be needed. We showed close agreement in measured levels over consecutive years at the same sites, except when strong temporary sources occurred in some sets (e.g., industrial exploration) or when more variable, biological sources dominated in some years.

The geographic grid size chosen for the model might affect the received levels in some cells and change the ship-to-wind noise ratio. We modelled on a 5 km $\times$ 5 km grid, and so the source cells were assigned a received level at 2.6 km range. A 2.5 km $\times$ 2.5 km grid would have a mean receiver range of 1.3 km. If ships are evenly distributed within a 5 km $\times$ 5 km cell, then halving the grid size will increase received levels within the source cells by 20 $\log_{10}(2)$ = 6 dB. The time spent in the source cell, however, will decrease by a factor 4, or, 10 $\log_{10}(4)$ = 6 dB, making up for the increase in received level (i.e., decrease in propagation range and thus, propagation loss). If ships are unevenly distributed within the larger grid cell, then changing to a finer grid will yield a net increase in modelled received noise levels within source cells. In comparison, the modelled noise levels from wind, being a sheet (rather than monopole) source, will not vary with grid size as wind speed changes on a much larger spatial scale offshore. Therefore, in areas where shipping lanes are well-defined and narrow (<5 km wide), ship noise levels may exceed wind noise levels by more than modelled in this article.

Based on our model and its 25-point validation, the Australian EEZ has a higher proportion of natural underwater noise from wind over ship noise than the North Sea and likely other northern hemisphere oceans [18,32]. Part of the Australian marine soundscape appears pristine, if pristine is defined as an absence of anthropogenic noise and a richness of biological noise (see also [78]). We have shown that accurate models of the Australian marine soundscape must include biological sources (i.e., primarily whales and fishes). Natural biological and physical noise ought to be considered in management frameworks to provide context (e.g., for noise management in the Southern Ocean [79]).

Our recommendations for future work include the establishment of a databank of Australian ship source spectra as started by [80], which will allow replacing the RANDI model with monopole source spectra from actual measurements. We have shown that other anthropogenic noise sources cannot be excluded in areas and years where these dominate and their contribution to the marine noise budget should be assessed. Comparing long-term cumulative sound exposure might not be the quantity most useful to managers. Instead, sound energy could be integrated over much shorter time frames and maps of % time above certain management thresholds be plotted [81], which is likely more relevant to biological

receptors than an annual or seasonal integral or average. The different sound sources have different acoustic features (e.g., ship and wind noise are continuous, while seismic surveying and pile driving are pulsed) and bioacoustic impact is likely driven by different acoustic quantities (e.g., sound exposure versus peak pressure [82]). Therefore, different quantities will have to be mapped for different types of impact. Moreover, these sources exhibit fundamentally different sound radiation fields, where an underwater explosion is a monopole, a ship is a dipole, pile driving a line source, and wind a sheet source, requiring different modelling approaches.

Supplementary Materials: The following are available online at https://www.mdpi.com/article/10.3390/jmse9050472/s1.

Author Contributions: Conceptualization, C.E., J.N.S. and D.P.; methodology, C.E.; software, C.E. and R.P.S.; formal analysis, C.E. and R.P.S.; data curation, C.E., D.P., J.N.S. and R.P.S.; writing—original draft preparation, C.E., R.P.S., D.P. and J.N.S.; writing—review and editing, C.E., R.P.S., D.P. and J.N.S.; visualization, C.E., D.P., J.N.S. and R.P.S.; project administration, D.P.; funding acquisition, D.P., J.N.S. and C.E. All authors have read and agreed to the published version of the manuscript.

Funding: This work was funded as part of the Australian National Environmental Science Programme, Marine Biodiversity Hub, under Project E2.

Institutional Review Board Statement: Not applicable.

Informed Consent Statement: Not applicable.

Data Availability Statement: A spreadsheet with the acoustic parameters that characterise each zone (i.e., mean winter sound speed profile; mean water depth and slope; sediment thickness; and compressional sound speed, shear sound speed, compressional absorption coefficient, shear absorption coefficient, and mean seafloor density) is available for download, as is a shape file of the spatially separated 28 acoustic zones (see https://tinyurl.com/3webp3pn). A spreadsheet with the sound speed profiles, water density profiles, and geoacoustic properties of the seafloor is available as Supplementary Material. Maps and data of cumulative sound exposure levels (C-SEL) from shipping over all ship classes in the Australian EEZ corresponding to Figure 6 can be found at Seamap Australia (https://seamapaustralia.org/; https://tinyurl.com/ahbs6nwr) and the AODN (https://catalogue.aodn.org.au/geonetwork/srv/eng/metadata.show?uuid=480847b4-b692-4112-89ff-0dcef75e3b84). Map and data of modelled wind noise from Figure 7 can also be found at Seamap Australia (https://tinyurl.com/a477j3b9) and the AODN (https://catalogue.aodn.org.au/geonetwork/srv/eng/metadata.show?uuid=0d3c7edc-463a-4fa0-8039-4d5a779035c3). All sites last accessed on: 30 March 2021.

Acknowledgments: We sincerely thank Robert D. McCauley for providing the sea noise data sets used for validation.

Conflicts of Interest: The authors declare no conflict of interest.

Appendix A

Step-by-step process of modelling ship noise:

1. Beginning with a GIS layer of the Australian marine bathymetry.
2. Add layers to the grid with ship positions, grouped by ship size (i.e., ship length), yielding one layer per ship class.
3. Split the EEZ grid into 28 previously determined acoustic zones.
4. For each zone:
    a. Find all grid cells that contain ships of any class, cast 36,100 km radials in 10-degree intervals, and extract bathymetry along the radials.
    b. Cluster all extracted bathymetries (over all radials around all cells with ships) with a neural network and subsequent k-means into 64 clusters.
    c. Compute sound propagation along each cluster centroid, for the centre frequencies of adjacent octave bands.
    d. For each ship size class:

i. Find the cells that contain ships of this class (source cells), cast 36,100 km radials in 10-degree intervals, and extract bathymetry along the radials.
ii. For each source cell:
- For each radial:
  - Look up into which cluster this radial went;
  - For each frequency:
    - Retrieve propagation loss as a function of range and depth.
    - Add octave band source level for this ship class.
    - Add cumulative time that a ship of this class spent in this source cell to yield sound exposure level as a function of range and depth.
    - Regrid from polar to Cartesian coordinates.

iii. Accumulate sound exposure over all radials and source cells to yield a 4-d matrix of cumulative sound exposure level as a function of longitude, latitude, depth, and frequency for each ship class.

e. Accumulate sound exposure over all ship classes.

5. Accumulate this 4-d matrix over all zones, EEZ-wide.
6. Sum over frequency to yield a 3-d matrix of cumulative sound exposure level as a function of longitude, latitude, and depth.
7. Pick the maximum cumulative sound exposure level over depth to yield a 2-d map of cumulative sound exposure level versus longitude and latitude.

References

1. Mahanty, M.M.; Sanjana, M.C.; Latha, G.; Raguraman, G. An investigation on the fluctuation and variability of ambient noise in shallow waters of south west Bay of Bengal. *Indian J. Geo Mar. Sci.* **2014**, *43*, 747–753.
2. Haver, S.M.; Fournet, M.E.H.; Dziak, R.P.; Gabriele, C.; Gedamke, J.; Hatch, L.T.; Haxel, J.; Heppell, S.A.; McKenna, M.F.; Mellinger, D.K.; et al. Comparing the underwater soundscapes of four U.S. National Parks and Marine Sanctuaries. *Front. Mar. Sci.* **2019**, *6*. [CrossRef]
3. Gage, S.H.; Axel, A.C. Visualization of temporal change in soundscape power of a Michigan lake habitat over a 4-year period. *Ecol. Inform.* **2014**, *21*, 100–109. [CrossRef]
4. Caruso, F.; Alonge, G.; Bellia, G.; De Domenico, E.; Grammauta, R.; Larosa, G.; Mazzola, S.; Riccobene, G.; Pavan, G.; Papale, E.; et al. Long-term monitoring of dolphin biosonar activity in deep pelagic water of the Mediterranean Sea. *Sci. Rep.* **2017**, *7*, 4321. [CrossRef]
5. Erbe, C.; Verma, A.; McCauley, R.; Gavrilov, A.; Parnum, I. The marine soundscape of the Perth Canyon. *Prog. Oceanogr.* **2015**, *137*, 38–51. [CrossRef]
6. McWilliam, J.N.; McCauley, R.D.; Erbe, C.; Parsons, M.J.G. Patterns of biophonic periodicity on coral reefs in the Great Barrier Reef. *Sci. Rep.* **2017**, *7*, 17459. [CrossRef]
7. Marley, S.A.; Erbe, C.; Salgado Kent, C.P.; Parsons, M.J.G.; Parnum, I.M. Spatial and temporal variation in the acoustic habitat of bottlenose dolphins (*Tursiops aduncus*) within a highly urbanised estuary. *Front. Mar. Sci.* **2017**, *4*, 197. [CrossRef]
8. McDonald, M.A.; Hildebrand, J.A.; Wiggins, S.M.; Ross, D. A 50 year comparison of ambient ocean noise near San Clemente Island: A bathymetrically complex coastal region off Southern California. *J. Acoust. Soc. Am.* **2008**, *124*, 1985–1992. [CrossRef]
9. European Commission. Future Noise Policy. Publications Office of the EU 1996, COM_1996_0540_FIN, Green Paper. Available online: https://op.europa.eu/en/publication-detail/-/publication/8d243fb5-ec92-4eee-aac0-0ab194b9d4f3/language-en (accessed on 15 March 2021).
10. European Commission. Directive 2002/49/EC of the European Parliament and of the Council relating to the assessment and management of environmental noise. *Off. J. Eur. Communities* **2002**, *L 189*, 12–25. Available online: https://eur-lex.europa.eu/legal-content/EN/TXT/PDF/?uri=CELEX:32002L0049&from=EN (accessed on 15 March 2021).
11. van der Graaf, A.J.; Ainslie, M.A.; Andre, M.; Brensing, K.; Dalen, J.; Dekeling, R.P.A.; Robinson, S.M.; Tasker, M.L.; Thomsen, F.; Werner, S. *European Marine Strategy Framework Directive—Good Environmental Status (MSFD GES): Report of the Technical Subgroup on Underwater Noise and Other Forms of Energy*; TSG Noise & Milieu Ltd.: Brussels, Belgium, 2012.
12. Erbe, C. Underwater noise from pile driving in Moreton Bay, Qld. *Acoust. Aust.* **2009**, *37*, 87–92.
13. Erbe, C.; King, A.R. Modelling cumulative sound exposure around marine seismic surveys. *J. Acoust. Soc. Am.* **2009**, *125*, 2443–2451. [CrossRef]

14. Farcas, A.; Thompson, P.M.; Merchant, N.D. Underwater noise modelling for environmental impact assessment. *Environ. Impact Assess. Rev.* **2016**, *57*, 114–122. [CrossRef]
15. Aulanier, F.; Simard, Y.; Roy, N.; Gervaise, C.; Bandet, M. Effects of shipping on marine acoustic habitats in Canadian Arctic estimated via probabilistic modeling and mapping. *Mar. Pollut. Bull.* **2017**, *125*, 115–131. [CrossRef] [PubMed]
16. Erbe, C.; MacGillivray, A.O.; Williams, R. Mapping cumulative noise from shipping to inform marine spatial planning. *J. Acoust. Soc. Am.* **2012**, *132*, EL423–EL428. [CrossRef] [PubMed]
17. Jalkanen, J.P.; Johansson, L.; Liefvendahl, M.; Bensow, R.; Sigray, P.; Östberg, M.; Karasalo, I.; Andersson, M.; Peltonen, H.; Pajala, J. Modelling of ships as a source of underwater noise. *Ocean Sci.* **2018**, *14*, 1373–1383. [CrossRef]
18. Sertlek, H.Ö.; Slabbekoorn, H.; ten Cate, C.; Ainslie, M.A. Source specific sound mapping: Spatial, temporal and spectral distribution of sound in the Dutch North Sea. *Environ. Pollut.* **2019**. [CrossRef] [PubMed]
19. Andrew, R.K.; Howe, B.M.; Mercer, J.A. Long-time trends in ship traffic noise for four sites off the North American West Coast. *J. Acoust. Soc. Am.* **2011**, *129*, 642–651. [CrossRef]
20. Andrew, R.; Bruce, M.H.; James, A.M. Ocean ambient sound: Comparing the 1960s with the 1990s for a receiver off the California coast. *Acoust. Res. Lett. Online* **2002**, *3*, 65–70. [CrossRef]
21. McDonald, M.A.; Hildebrand, J.A.; Wiggins, S.M. Increases in deep ocean ambient noise in the Northeast Pacific west of San Nicolas Island, California. *J. Acoust. Soc. Am.* **2006**, *120*, 711–718. [CrossRef] [PubMed]
22. Chapman, N.R.; Price, A. Low frequency deep ocean ambient noise trend in the Northeast Pacific Ocean. *J. Acoust. Soc. Am.* **2011**, *129*, EL161–EL165. [CrossRef] [PubMed]
23. Miksis-Olds, J.L.; Bradley, D.L.; Niu, X.M. Decadal trends in Indian Ocean ambient sound. *J. Acoust. Soc. Am.* **2013**, *134*, 3464–3475. [CrossRef]
24. Miksis-Olds, J.L.; Nichols, S.M. Is low frequency ocean sound increasing globally? *J. Acoust. Soc. Am.* **2016**, *139*, 501–511. [CrossRef]
25. Erbe, C.; Marley, S.; Schoeman, R.; Smith, J.N.; Trigg, L.; Embling, C.B. The effects of ship noise on marine mammals—A review. *Front. Mar. Sci.* **2019**, *6*, 606. [CrossRef]
26. Ferrari, M.C.O.; McCormick, M.I.; Meekan, M.G.; Simpson, S.D.; Nedelec, S.L.; Chivers, D.P. School is out on noisy reefs: The effect of boat noise on predator learning and survival of juvenile coral reef fishes. *Proc. Biol. Sci.* **2018**, *285*. [CrossRef] [PubMed]
27. Kusku, H. Acoustic sound–induced stress response of Nile tilapia (*Oreochromis niloticus*) to long-term underwater sound transmissions of urban and shipping noises. *Environ. Sci. Pollut. Res.* **2020**. [CrossRef]
28. Williams, R.; Cholewiak, D.; Clark, C.W.; Erbe, C.; George, J.C.C.; Lacy, R.C.; Leaper, R.; Moore, S.E.; New, L.; Parsons, E.C.M.; et al. Chronic ocean noise and cetacean population models. *J. Cetacean Res. Manag.* **2020**, *21*, 85–94. [CrossRef]
29. Erbe, C.; Williams, R.; Sandilands, D.; Ashe, E. Identifying modelled ship noise hotspots for marine mammals of Canada's Pacific region. *PLoS ONE* **2014**, *9*, e89820. [CrossRef] [PubMed]
30. Williams, R.; Erbe, C.; Ashe, E.; Clark, C.W. Quiet(er) marine protected areas. *Mar. Pollut. Bull.* **2015**, *100*, 154–161. [CrossRef]
31. Jensen, F.B.; Kuperman, W.A.; Porter, M.B.; Schmidt, H. *Computational Ocean Acoustics*, 2nd ed.; Springer: New York, NY, USA, 2011.
32. Farcas, A.; Powell, C.F.; Brookes, K.L.; Merchant, N.D. Validated shipping noise maps of the Northeast Atlantic. *Sci. Total Environ.* **2020**, *735*, 139509. [CrossRef]
33. Wu, L.; Xu, Y.; Wang, Q.; Wang, F.; Xu, Z. Mapping global shipping density from AIS data. *J. Navig.* **2017**, *70*, 67–81. [CrossRef]
34. McCauley, R.D.; Gavrilov, A.N.; Jolliffe, C.D.; Ward, R.; Gill, P.C. Pygmy blue and Antarctic blue whale presence, distribution and population parameters in southern Australia based on passive acoustics. *Deep Sea Res. Part II Top. Stud. Oceanogr.* **2018**. [CrossRef]
35. Dawbin, W.H. The seasonal migratory cycle of humpback whales. In *Whales, Dolphins and Porpoises*; Norris, K.S., Ed.; University of California Press: Berkeley, CA, USA, 1966; pp. 145–170.
36. Bannister, J. Status of southern right whales (*Eubalaena australis*) off Australia. *J. Cetacean Res. Manag.* **2020**, 103–110. [CrossRef]
37. Erbe, C.; Peel, D.; Smith, J.N.; Schoeman, R.P. Marine acoustic zones of Australia. *J. Mar. Sci. Eng.* **2021**, *9*, 340. [CrossRef]
38. Whiteway, T.G. *Australian Bathymetry and Topography Grid*; 2009/21; Geoscience Australia: Canberra, Australia, 2009.
39. Peel, D.; Erbe, C.; Smith, J.N.; Parsons, M.J.G.; Duncan, A.J.; Schoeman, R.P.; Meekan, M. *Characterising Anthropogenic Underwater Noise to Improve Understanding and Management of Acoustic Impacts to Marine Wildlife*; CSIRO: Hobart, Australia, 2021.
40. Breeding, J.E.; Pflug, L.A.; Bradley, M.; Herbert, M.; Wooten, M. *RANDI 3.1 User's Guide*; Naval Research Laboratory: Washington, DC, USA, 1994.
41. Durrant, T.; Hemer, M.; Trenham, C.; Greenslade, D. *CAWCR Wave Hindcast Extension Jan 2011–May 2013. v7*; CSIRO Service Collection: Canberra, Australia, 2013.
42. Saha, S.; Moorthi, S.; Wu, X.; Wang, J.; Nadiga, S.; Tripp, P.; Behringer, D.; Hou, Y.-T.; Chuang, H.-y.; Iredell, M.; et al. The NCEP Climate Forecast System Version 2. *J. Clim.* **2014**, *27*, 2185–2208. [CrossRef]
43. Wenz, G.M. Acoustic ambient noise in the ocean: Spectra and sources. *J. Acoust. Soc. Am.* **1962**, *34*, 1936–1956. [CrossRef]
44. Mathai, A.; Moschopoulos, P.; Pederzoli, G. Random points associated with rectangles. *Rend. Circ. Mat. Palermo* **1999**, *48*, 163–190. [CrossRef]
45. Vesanto, J.; Himberg, J.; Alhoniemi, E.; Parhankangas, J. *SOM Toolbox for Matlab 5*; Helsinki University of Technology: Helsinki, Finland, 2000.

46. Vesanto, J.; Alhoniemi, E. Clustering of the self-organizing map. *IEEE Trans. Neural Netw.* **2000**, *11*, 586–600. [CrossRef] [PubMed]
47. Duncan, A.; Maggi, A.L. A consistent, user friendly interface for running a variety of underwater acoustic propagation codes. In Proceedings of the Acoustics 2006, Christchurch, New Zealand, 20–22 November 2006.
48. Locarnini, R.A.; Mishonov, A.V.; Baranova, O.K.; Boyer, T.P.; Zweng, M.M.; Garcia, H.E.; Reagan, J.R.; Seidov, D.; Weathers, K.; Paver, C.R.; et al. *World Ocean Atlas 2018, Volume 1: Temperature*; National Oceanic and Atmospheric Administration: Washington, DC, USA, 2018.
49. Zweng, M.M.; Reagan, J.R.; Seidov, D.; Boyer, T.P.; Locarnini, R.A.; Garcia, H.E.; Mishonov, A.V.; Baranova, O.K.; Weathers, K.; Paver, C.R.; et al. *World Ocean Atlas 2018, Volume 2: Salinity*; National Oceanic and Atmospheric Administration: Washington, DC, USA, 2018.
50. Fofonoff, N.P.; Millard, R.C., Jr. *Algorithms for the Computation of Fundamental Properties of Seawater*; UNESCO Technical Papers in Marine Sciences; UNESCO: Paris, France, 1983; Volume 44.
51. Duncan, A.; Gavrilov, A.; Li, F. Acoustic propagation over limestone seabeds. In Proceedings of the Acoustics 2009, Adelaide, Australia, 23–25 November 2009.
52. Torgersen, T.; Jones, M.R.; Stephens, A.W.; Searle, D.E.; Ullman, W.J. Late Quaternary hydrological changes in the Gulf of Carpentaria. *Nature* **1985**, *313*, 785–787. [CrossRef]
53. Jones, M.R.; Torgersen, T. Late Quaternary evolution of Lake Carpentaria on the Australia-New Guinea continental shelf. *Aust. J. Earth Sci.* **1988**, *35*, 313–324. [CrossRef]
54. Roy, P.S.; Cowell, P.J.; Ferland, M.A.; Thom, B.G. Wave-dominated coasts. In *Coastal Evolution: Late Quaternary Shoreline Morphodynamics*; Woodroffe, C.D., Carter, R.W.G., Eds.; Cambridge University Press: Cambridge, UK, 1995; pp. 121–186. [CrossRef]
55. Heap, A.; Daniell, J.; Mazen, D.; Harris, P.; Sbaffi, L.; Fellows, M.; Passlow, V. *Geomorphology and Sedimentology of the Northern Marine Planning Area of Australia: Review and Synthesis of Relevant Literature in Support of Regional Marine Planning*; 2004/11; Geoscience Australia: Canberra, Australia, 2004.
56. Carter, R.M.; Larcombe, P.; Dye, J.E.; Gagan, M.K.; Johnson, D.P. Long-shelf sediment transport and storm-bed formation by Cyclone Winifred, central Great Barrier Reef, Australia. *Mar. Geol.* **2009**, *267*, 101–113. [CrossRef]
57. Harris, P.T.; Heap, A.D. Cyclone-induced net sediment transport pathway on the continental shelf of tropical Australia inferred from reef talus deposits. *Cont. Shelf Res.* **2009**, *29*, 2011–2019. [CrossRef]
58. Koessler, M.W. An equivalent fluid representation of a layered elastic seafloor for acoustic propagation modelling. In Proceedings of the Acoustics 2017, Perth, Australia, 19–22 November 2017.
59. Porter, M.B. *The KRAKEN Normal Mode Program*; NRL/MR/5120-92-6920; Naval Research Laboratory: Washington, DC, USA, 1992.
60. Fisher, F.H.; Simmons, V.P. Sound absorption in sea water. *J. Acoust. Soc. Am.* **1977**, *62*, 558–564. [CrossRef]
61. Schreer, J.F.; Kovacs, K.M. Allometry of diving capacity in air-breathing vertebrates. *Can. J. Zool.* **1997**, *75*, 339–358. [CrossRef]
62. McCauley, R.D.; Thomas, F.; Parsons, M.J.G.; Erbe, C.; Cato, D.; Duncan, A.J.; Gavrilov, A.N.; Parnum, I.M.; Salgado-Kent, C. Developing an underwater sound recorder. *Acoust. Aust.* **2017**, *45*, 301–311. [CrossRef]
63. Gavrilov, A.N.; Parsons, M.J.G. A Matlab tool for the characterisation of recorded underwater sound (CHORUS). *Acoust. Aust.* **2014**, *42*, 190–196.
64. Erbe, C.; McCauley, R.; Gavrilov, A.; Madhusudhana, S.; Verma, A. The underwater soundscape around Australia. In Proceedings of the Acoustics 2016, Brisbane, Australia, 9–11 November 2016.
65. Erbe, C.; Dunlop, R.; Jenner, K.C.S.; Jenner, M.-N.M.; McCauley, R.D.; Parnum, I.; Parsons, M.; Rogers, T.; Salgado-Kent, C. Review of underwater and in-air sounds emitted by Australian and Antarctic marine mammals. *Acoust. Aust.* **2017**, *45*, 179–241. [CrossRef]
66. McWilliam, J.N.; McCauley, R.D.; Erbe, C.; Parsons, M.J.G. Soundscape diversity in the Great Barrier Reef: Lizard Island, a case study. *Bioacoustics* **2018**, *27*, 295–311. [CrossRef]
67. Ward, R.; Gavrilov, A.N.; McCauley, R.D. "Spot" call: A common sound from an unidentified great whale in Australian temperate waters. *J. Acoust. Soc. Am.* **2017**, *142*, EL231–EL236. [CrossRef]
68. MacGillivray, A.O.; Li, Z.; Hannay, D.E.; Trounce, K.B.; Robinson, O.M. Slowing deep-sea commercial vessels reduces underwater radiated noise. *J. Acoust. Soc. Am.* **2019**, *146*, 340–351. [CrossRef] [PubMed]
69. MacGillivray, A.; de Jong, C. A reference spectrum model for estimating source levels of marine shipping based on Automated Identification System data. *J. Mar. Sci. Eng.* **2021**, *9*, 369. [CrossRef]
70. Chion, C.; Lagrois, D.; Dupras, J.; Turgeon, S.; McQuinn, I.H.; Michaud, R.; Ménard, N.; Parrott, L. Underwater acoustic impacts of shipping management measures: Results from a social-ecological model of boat and whale movements in the St. Lawrence River Estuary (Canada). *Ecol. Model.* **2017**, *354*, 72–87. [CrossRef]
71. Jiang, P.; Lin, J.; Sun, J.; Yi, X.; Shan, Y. Source spectrum model for merchant ship radiated noise in the Yellow Sea of China. *Ocean Eng.* **2020**, *216*, 107607. [CrossRef]
72. Simard, Y.; Roy, N.; Gervaise, C.; Giard, S. Analysis and modeling of 255 source levels of merchant ships from an acoustic observatory along St. Lawrence Seaway. *J. Acoust. Soc. Am.* **2016**, *140*, 2002–2018. [CrossRef] [PubMed]
73. Erbe, C.; Liong, S.; Koessler, M.W.; Duncan, A.J.; Gourlay, T. Underwater sound of rigid-hulled inflatable boats. *J. Acoust. Soc. Am.* **2016**, *139*, EL223–EL227. [CrossRef] [PubMed]

74. Kipple, B.; Gabriele, C. *Glacier Bay Watercraft Noise*; NSWCCD-71-TR-2003/522; Naval Surface Warfare Center: Bremerton, WA, USA, 2003.
75. Kipple, B.; Gabriele, C. Underwater noise from skiffs to ships. In Proceedings of the Fourth Glacier Bay Science Symposium, Juneau, AK, USA, 26–28 October 2004; Piatt, J.F., Gende, S.M., Eds.; U.S. Geological Survey Scientific Investigations Report 2007-5047: Juneau, AL, USA, 2007; pp. 172–175.
76. Gervaise, C.; Simard, Y.; Roy, N.; Kinda, B.; Menard, N. Shipping noise in whale habitat: Characteristics, sources, budget, and impact on belugas in Saguenay–St. Lawrence Marine Park hub. *J. Acoust. Soc. Am.* **2012**, *132*, 76–89. [CrossRef]
77. Cato, D.H. Ocean ambient noise: Its measurement and its significance to marine animals. In Proceedings of the Institute of Acoustics—Underwater Noise Measurement, Impact and Mitigation, Southampton, UK, 14–15 October 2008; pp. 1–9.
78. Marley, S.A.; Salgado Kent, C.P.; Erbe, C.; Thiele, D. A tale of two soundscapes: Comparing the acoustic characteristics of urban versus pristine coastal dolphin habitats in Western Australia. *Acoust. Aust.* **2017**, *45*, 159–178. [CrossRef]
79. Erbe, C.; Dähne, M.; Gordon, J.; Herata, H.; Houser, D.S.; Koschinski, S.; Leaper, R.; McCauley, R.; Miller, B.; Müller, M.; et al. Managing the effects of noise from ship traffic, seismic surveying and construction on marine mammals in Antarctica. *Front. Mar. Sci.* **2019**. [CrossRef]
80. Erbe, C.; Duncan, A.; Peel, D.; Smith, J.N. *Underwater Noise Signatures of Ships in Australian Waters*; Centre for Marine Science and Technology, Curtin University: Hobart, Australia, 2020.
81. Merchant, N.D.; Faulkner, R.C.; Martinez, R. Marine noise budgets in practice. *Conserv. Lett.* **2018**, *11*, e12420. [CrossRef]
82. Southall, B.L.; Finneran, J.J.; Reichmuth, C.; Nachtigall, P.E.; Ketten, D.R.; Bowles, A.E.; Ellison, W.T.; Nowacek, D.P.; Tyack, P.L. Marine mammal noise exposure criteria: Updated scientific recommendations for residual hearing effects. *Aquat. Mamm.* **2019**, *45*, 125–232. [CrossRef]